大環状ポリアミン亜鉛錯体による
選択的核酸塩基認識と遺伝子発現制御

2001

木下恵美子

Sequence Selective Recognition of DNA and Controlling Gene Expression by Zinc(II)–Macrocyclic Tetraamine Complexes

2001

Emiko Kinoshita

CONTENTS

Introduction

Small molecules recognizing specific DNA sequence have attracted great interest for gene-targeted drugs, which may alter the local structure of DNA to inhibit access of activators or repressors to regulate ultimate gene expression processes.[1-2] A number of clinically useful drugs such as distamycin A (**1**),[3-10] 4,6-diamidino-2-phenylindole (DAPI) (**2**),[8-9,11-15] echinomycin (**3**),[16-19] actinomycin D (**4**),[4-6,20-23] and cisplatin[24-32] interact with DNA in various fashions via hydrophobic, electrostatic, hydrogen-bonding, dipolar forces, and/or coordinate interactions. Of these, distamycin A and DAPI are minor groove binders that recognize AT-rich regions. They simultaneously bind to adenine N(3) and thymine O(2) by hydrogen bondings and stabilize the A-T duplex structure (Scheme 1).[3-15] Other drugs equipped with intercalators such as actinomycin D,[4-6,20-23] or metallointercalators[33] bind to GC-rich regions of DNA. Either type of DNA-recognizing molecules is useful in perturbing some stage of transcription processes. An anticancer platinum compound, *cis*-platin coordinates mainly to 1,2-intrastrand guanines.[24-32] Currently, chemical modification of these drugs has been actively undertaken.[34-37]

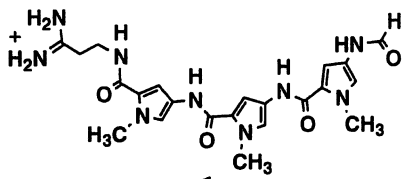

1
Distamycin A

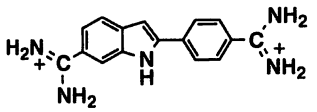

2
DAPI
(4,6-diamidino-2-phenylindole)

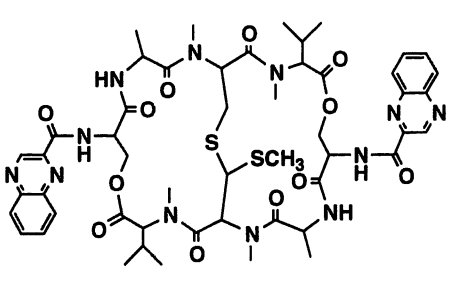

3
Echinomycin

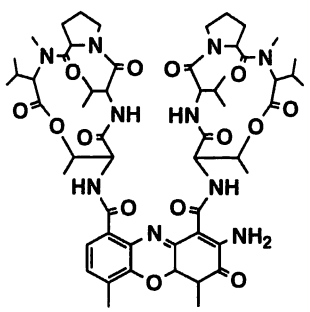

4
Actinomycin D

Scheme 1

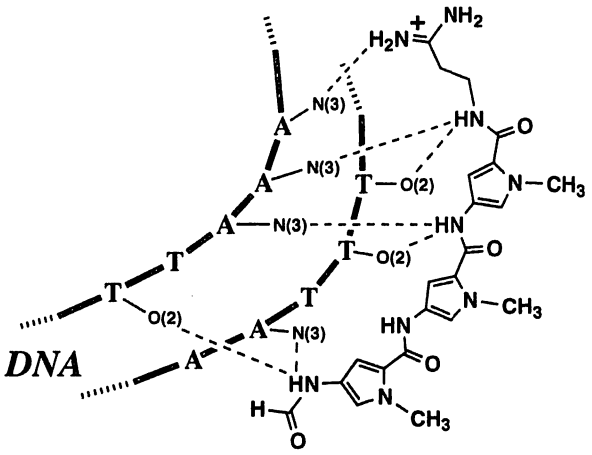

minor groove binding
by distamycin A

Recently, some macrocyclic tetraamine zinc(II) complexes, Zn^{2+}–cyclen (**5**) (cyclen = 1,4,7,10-tetraazacyclododecane),[38] was found to selectively bind to deoxythymidine (dT) and uridine (U) in aqueous solution at physiological pH with disassociation constants K_d = 0.3 mM and 0.8 mM (at pH 8), respectively (Scheme 2). In the resulting ternary complexes **6**, the nucleobases take N(3)-deprotonated anionic form (dT^- or U^-) to bind with Zn^{2+}. Moreover, Zn^{2+}–(9-acridinyl)methyl-cyclen (= Zn^{2+}–acridinylcyclen, (**7**))[39] bound to dT and U to form **8** with higher affinity than **5** (K_d = 16 μM and 32 μM (at pH 8)), respectively due to hydrophobic (π-π stacking) interaction between the two aromatic rings.

In addition, **7** showed an appreciably strong association with neutral deoxyguanosine (dG) to form **9** through a Zn^{2+}–N(7)(guanine) coordination, a hydrogen bond between the cyclen NH and O(6)(guanine), and a hydrophobic interaction between the two aromatic rings.[39] Further, **7** appeared to interact with guanine base in double-stranded poly(dG)·poly(dC), probably by major groove binding and intercalation to stabilize the double-stranded structure , as indicated by the higher T_m.[40-41]

More recently, a *p*-bis(Zn^{2+}–cyclen) (**10**) and a *p*-tris(Zn^{2+}–cyclen) (**11**) were found to selectively bind to a dinucleotide dTpdT and a trinucleotide dTpdTpdT, with extremely small dissociation constants K_d = 0.6 μM and 0.8 nM (at pH 7.4), respectively (Scheme 3).[42-43]

In order to find a more detailed T-recognizing picture on DNA, we now have adopted biochemical approach. With the use of well-established DNA nucleases footprinting analysis technique,[44-46] we revealed the sequence-selective properties of the Zn^{2+}–cyclen derivatives. In our efforts to make a further development on the basis of the novel chemistry involving the

Zn^{2+}–cyclen derivatives and DNA, we have investigated the effects on biological reactions such as the Zn^{2+}–cyclen interaction to a promoter element for eukaryotic gene and inhibition of transcriptional factor, DNA topoisomerases or RNA polymerase inhibition, and antimicrobial activities.

Scheme 2

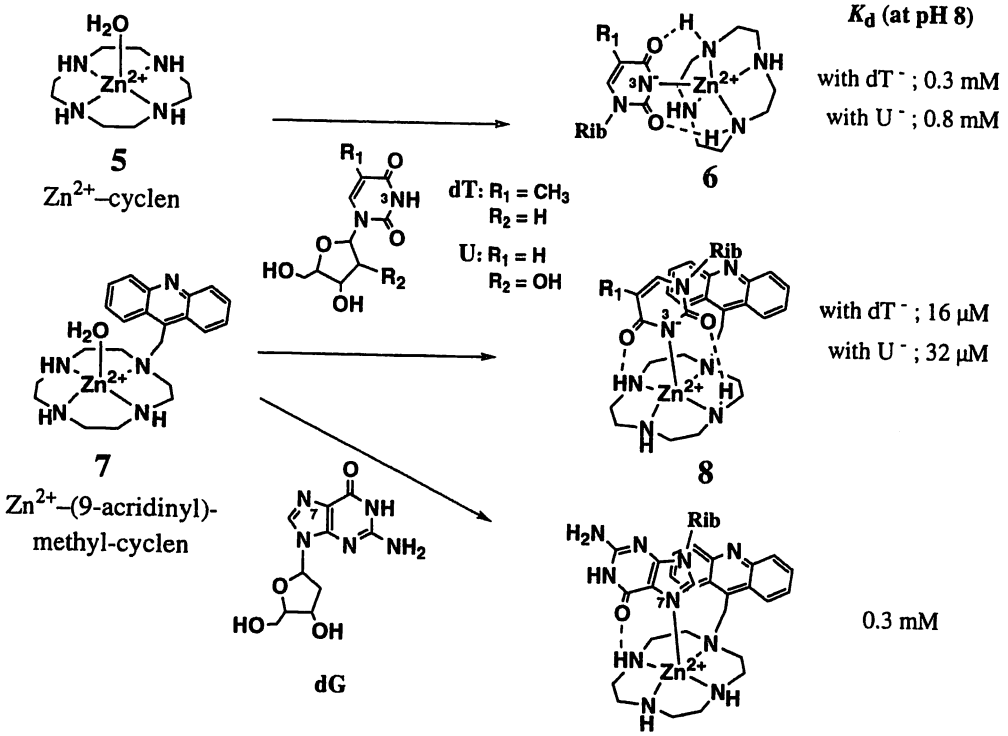

Scheme 3

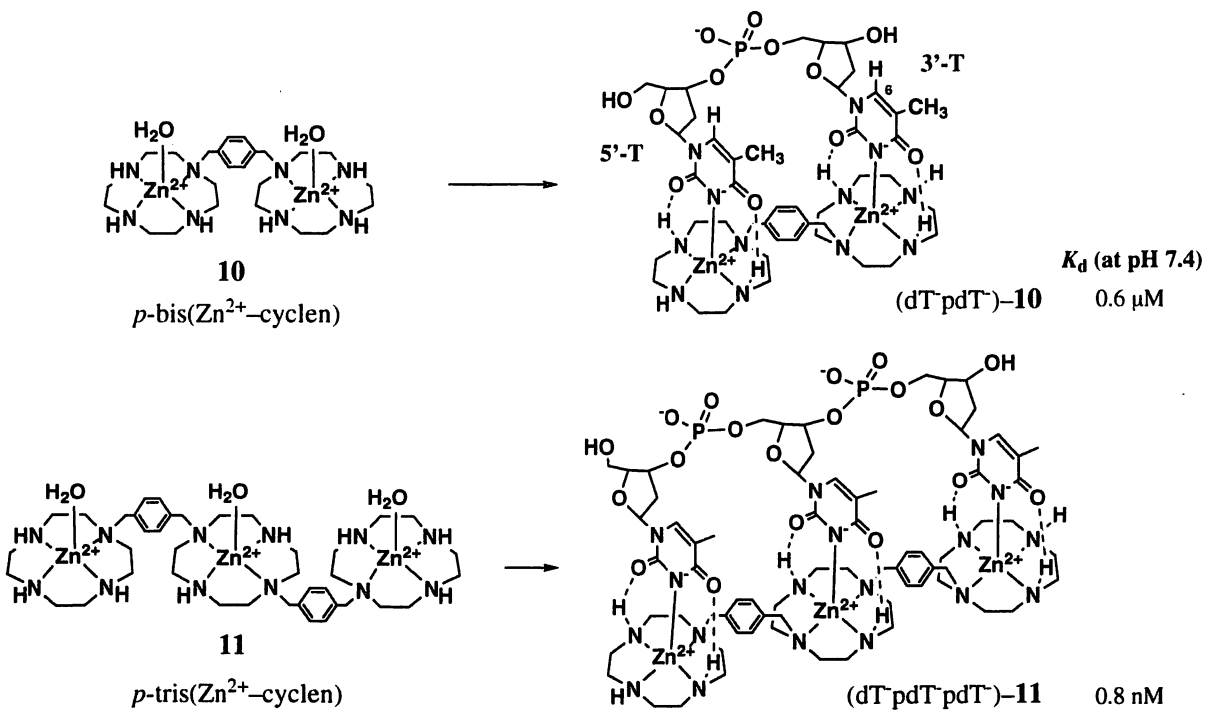

I Novel recognition of thymine base in double-stranded DNA by zinc(II)–macrocyclic tetraamine complexes appended with aromatic groups

1. Identification of the aromatic Zn^{2+}–cyclen derivatives binding sites on DNA

In the present study, we have newly synthesized Zn^{2+}–cyclen derivatives appended with polyaromatic quinoline or naphtalene groups, Zn^{2+}–(4-quinolyl)methyl-cyclen (= Zn^{2+}–quinolylcyclen, **12**), Zn^{2+}–1,7-bis((4-quinolyl)methyl)-cyclen (= Zn^{2+}–bisquinonylcyclen, **13**), Zn^{2+}–(1-naphthyl)methyl-cyclen (= Zn^{2+}–naphthylcyclen, **14**), and Zn^{2+}–1,7-bis((1-naphthyl)methyl)-cyclen (= Zn^{2+}–bisnaphthylcyclen, **15**), in the hope that some of Zn^{2+}–cyclen derivatives might better efficiently recognize T-sequence in double-stranded DNA than the previously synthesized Zn^{2+}–acridinylcyclen (**7**). Among these, **13** and **15** were somewhat similar to quinoxaline antibiotics, echinomycin (**3**), which strongly binds to DNA because of double stacking of two aromatic rings.

12

Zn^{2+}–(4-quinolyl)methyl-cyclen

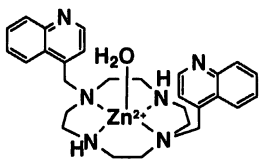

13

Zn^{2+}–1,7-bis((4-quinolyl)methyl)-cyclen

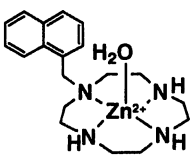

14

Zn^{2+}–(1-naphthyl)methyl-cyclen

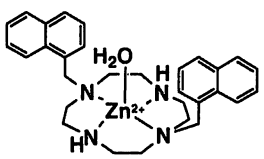

15

Zn^{2+}–1,7-bis((1-naphthyl)methyl)-cyclen

The conditional affinity constants of **12** – **15** with dT^- and dG, $K_{app}(ZnL–dT^-)$ = $[ZnL–dT^-]/[ZnL][\text{unbound dT}]$ (M^{-1}) and $K_{app}(ZnL–dG)$ = $[ZnL–dG]/[ZnL][\text{unbound dG}]$ (M^{-1}), respectively, were determined for pH 8 by almost the same potentiometric pH-titration method (at 25°C with I = 0.05 ($NaNO_3$)) as previously reported (see Appendix in p.57).[47-49] The obtained $K_{app}(ZnL–dT^-)$ values are around 10^4 – 10^5 M^{-1} (i.e., dissociation constants K_d = ca. 10 - 100 μM), as summarized in Table 1. Due to insufficient solubility for the potentiometric pH-titration in aqueous solution, the $K_{app}(ZnL–dT^-)$ and $K_{app}(ZnL–dG)$ value for **15** could not be determined.

Table 1 Comparison of the conditional affinity constants log K_{app}(ZnL–dT$^-$) and log K_{app}(ZnL–dG)[a] at pH 8.0 and 25 °C.

ZnL	log K_{app}(ZnL–dT$^-$)	log K_{app}(ZnL–dG)
5[b]	3.5	<2
7[c]	4.8	3.5
12[d]	4.3	2.4
13[d]	5.0	2.8
14[d]	4.2	2.4
15[e]	ND	ND

[a] K_{app}(ZnL–dT$^-$) = [ZnL–dT$^-$]/[ZnL][unbound dT] (M^{-1}), K_{app}(ZnL–dG) = [ZnL–dG]/[ZnL][unbound dG] (M^{-1}). The estimated error in the log K_{app}(ZnL–dT$^-$) and log K_{app}(ZnL–dG) values was ± 5%. [b] From ref 38 with I = 0.10 ($NaClO_4$). [c] From ref 39 with I = 0.10 ($NaNO_3$). [d] With I = 0.05 ($NaNO_3$). [e] Due to insufficient solubility in aqueous solution, log K_{app}(ZnL–dT$^-$) and log K_{app}(ZnL–dG) values could not be determined.

The binding sites of Zn^{2+}–cyclen derivatives **7**, **12**, **13**, **14**, and **15** (at concentrations 7.5 – 60 μM) on the 5'-^{32}P labeled DNA fragments from plasmid pUC19 (150 base pairs, the sequence is shown in Figure 2) have been analyzed first by DNase I footprinting method. The patterns of the DNase I digestion are shown in Figure 1 for the upper (Watson*) and lower (Crick*) strands. For comparison, minor groove binders distamycin A (**1**) (0.625 – 1.25 μM) and DAPI (**2**) (1.25 – 2.5 μM), which bind to AT-rich regions,[3-15,45] and a bis-intercalater echinomycin (**3**) (2.5 – 5 μM) that recognizes GC-rich regions,[16-19] were also tested side by side.

It is immediately apparent that all of the protected regions with the Zn^{2+}–cyclen derivatives (**7**, **12**, **13**, **14**, and **15**) are similar to those observed by distamycin A (**1**) and DAPI (**2**), but dissimilar to those by echinomycin (**3**). The interaction with GC-rich regions if any, on the other hand, would not be so strong as to hinder the DNase I attack. The acridine derivative **7** (e.g., 93 – 100 on the Crick strand) and bis-quinoline derivative **13** (e.g., 62 – 67 on the Watson strand) seemed to have minor interaction with GC-regions. Although there were some disparities between protected regions by the Zn^{2+}–cyclen derivatives and by the minor groove binders **1** and **2** (e.g., around 60), characteristically common protected sites are clearly discerned, located in the vicinity of the positions 48 and 80 on the Watson strand, and 80 and 105 on the Crick strand (see Figure 1). All of these common protected zones are associated with homopolymeric AT-region in the DNA

sequence, which appeared well defined in the differential cleavage plots (see Figure 2). Such protection was not observed with Zn^{2+}–cyclen **5** even at 100 μM concentration, implying that the aromatic rings are essential for the Zn^{2+}–cyclen part to interact with the DNA.

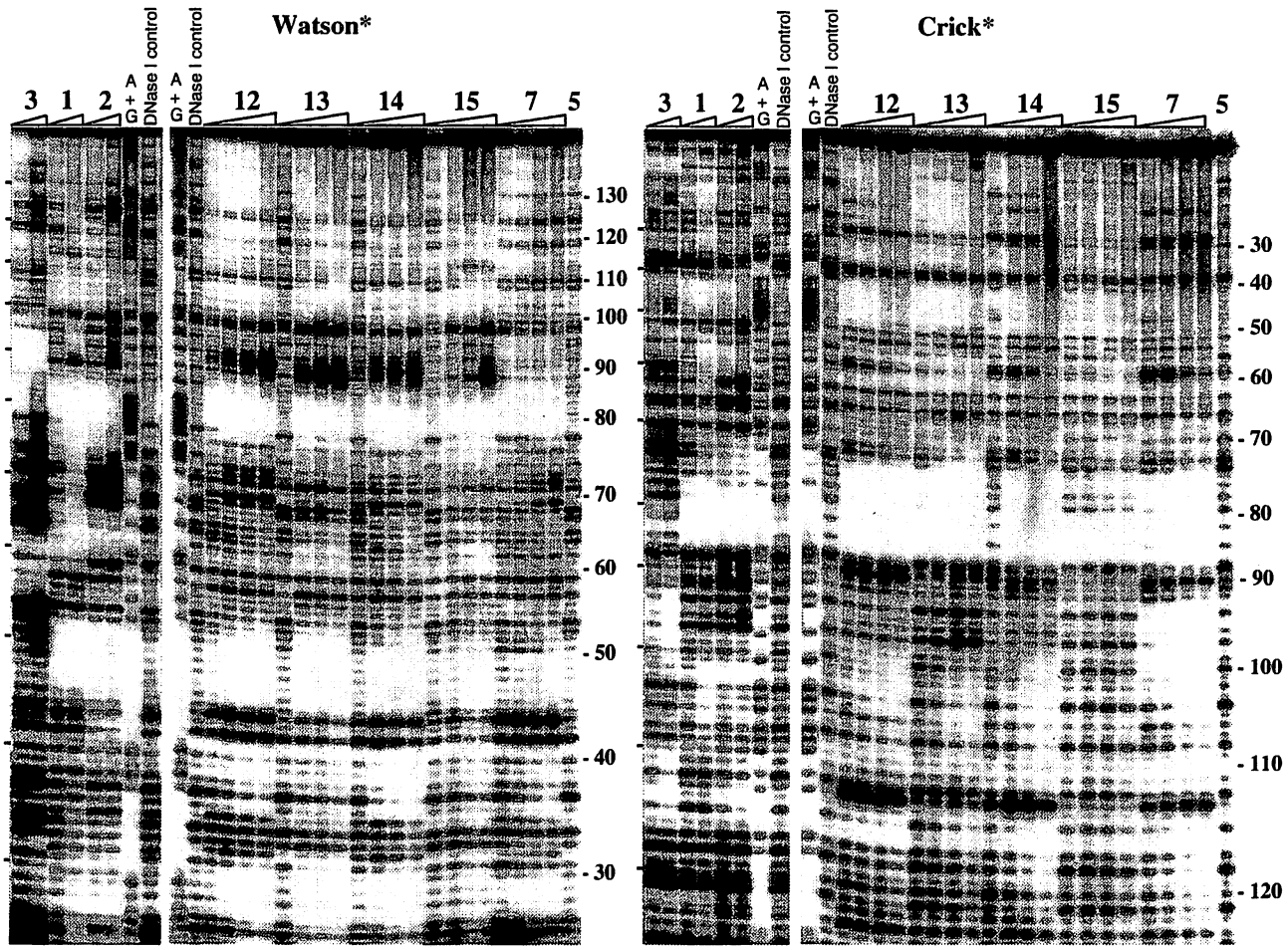

Figure 1 DNase I footprinting of 150 bp DNA in the presence of **1** (0.625 and 1.25 μM), **2** (1.25 and 2.5 μM), **3** (2.5 and 5 μM), **5** (100 μM), **7** (5, 7.5, 10, and 12.5 μM), **12** (30, 40, 50, and 60 μM), **13** (7.5, 10, 12.5, and 15 μM), **14** (20, 30, 40, and 50 μM), **15** (5, 7.5, 10, and 12.5 μM). Hereafter, the asterisk indicates which strand bears the 5'-^{32}P label (Watson* = upper strand, Crick* = lower strand shown in Figure 2). The lane "A+G" represents the Maxam-Gilbert sequencing marker specific for A and G. The lane "DNase I control" represents DNA digested with DNase I without binders. The number at the side corresponds to the sequence number shown in Figure 2.

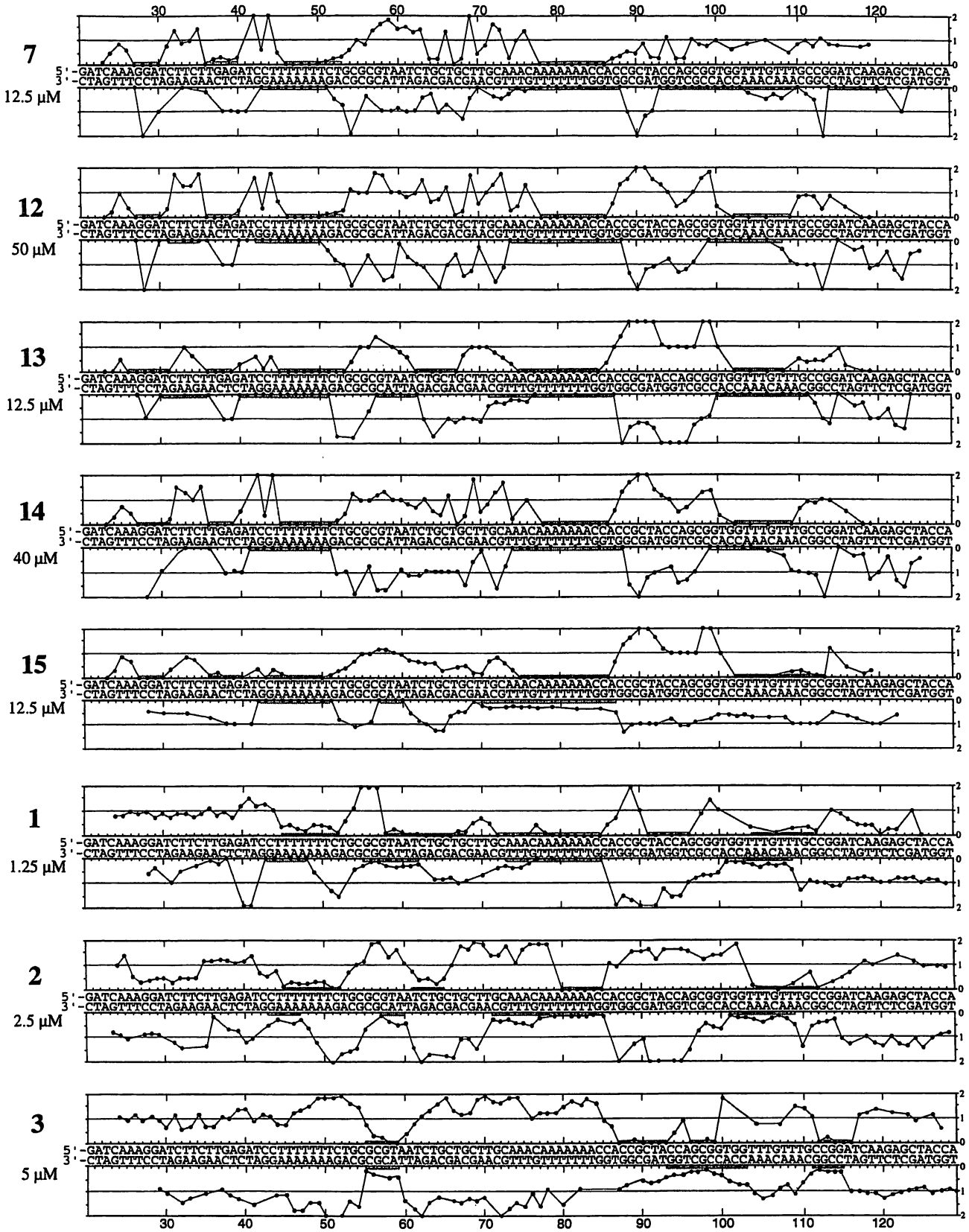

Figure 2 Differential DNase I cleavage plots in the presence of binders **7** (12.5 μM), **12** (50 μM), **13** (12.5 μM), **14** (40 μM), **15** (12.5 μM), **1** (1.25 μM), **2** (2.5 μM), and **3** (5.0 μM). The vertical scale corresponds to the ratio D/D_0, where D is the density of the band in the presence of a binder and D_0 in its absence.

Binding affinities and specificities varied with the kind or number of aromatic rings appended to the Zn^{2+}–cyclen. Among those active species, **7**, **13**, and **15** having higher log K_{app} values with dT (Table 1) showed the stronger binding with DNA. The evaluation came from the IC_{50} values, half the concentration required to inhibit the DNase I hydrolysis at TpTpTpTpTpTpT (45 – 50) in the Watson strand, which were determined by the footprinting titration (see Figure 3) and the results summarized in Table 2. Although their IC_{50} values (8 – 30 μM) were not as small as those for 0.5 μM distamycin A (**1**) and 2 μM DAPI (**2**), we think these values to be significant for the starting prototype. Similar IC_{50} values were seen for **12** and **14** (25 – 30 μM), and for **13** and **15** (8 – 9 μM). The DNase I digestion patterns were somewhat different between **12** and **13**, and between **14** and **15**. This may result from difference in the 'single-stacking' by the single aromatic pendants vs. 'double-stacking' binding mode by the double aromatic pendants.[50] The DNase I cleavage pattern of **7** was similar to those by **12** and **14**, although its IC_{50} value was higher and similar to those for **13** and **15**.

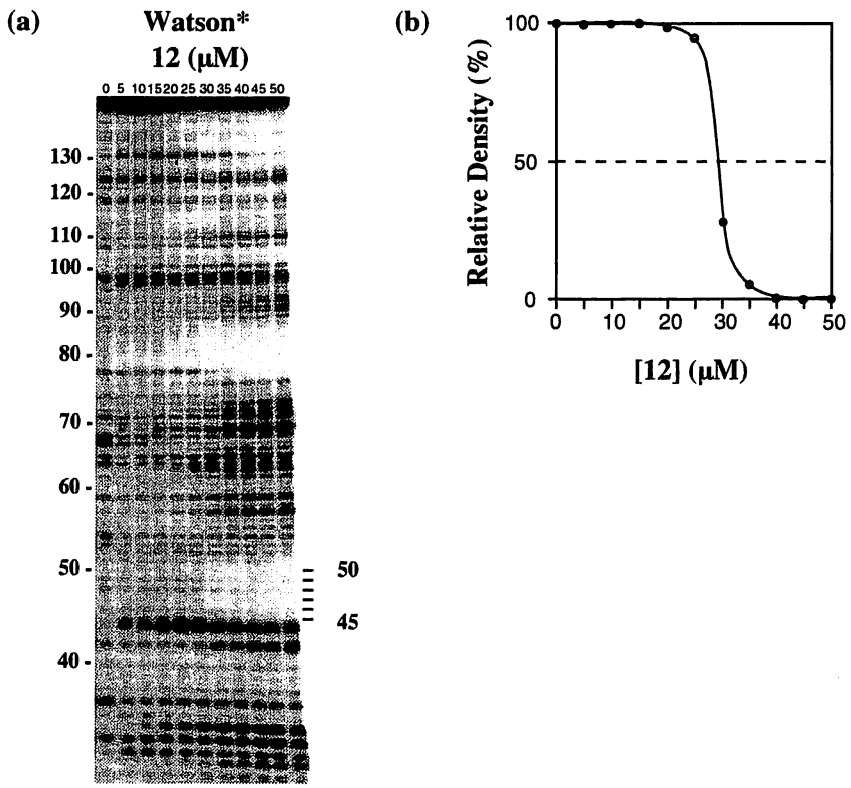

Figure 3 (a) DNase I footprinting titration with **12** (0 – 50 μM) on the 5'-^{32}P labeled Watson strand. (b) Footprinting titration plots of total density for the TpTpTpTpTpTpT moiety at 45 – 50. Relative density corresponds to the ratio D/D_0, where D is the total density of the six bands in the presence of **12** and D_0 in its absence.

Table 2 Half the concentration values (IC_{50})[a] of Zn^{2+}–cyclen derivatives (**7**, **12**, **13**, **14**, and **15**) and minor groove binders (**1** and **2**) required to inhibit the DNase I hydrolysis at TpTpTpTpTpTpT (45 – 50) in the Watson strand.

	IC_{50} (μM)
7	8
12	30
13	9
14	25
15	8
1	0.5
2	2

[a] The estimated error in the IC_{50} values was ± 10%.

The footprinting technique using hydroxy radicals (e.g., by Fe^{2+}–EDTA) is often employed to elucidate the groove and sequence preference of DNA binding molecules.[4,5,51-52] The footprinting with Fe^{2+}–EDTA ([Fe^{2+}] = 10 μM and [EDTA] = 20 μM), which gave anticipated DNA cleavage patterns in the absence and presence of distamycin A, was carried out in the presence of the Zn^{2+}–cyclen derivatives (0 – 100 μM). However, little cleavage of DNA occurred with increasing concentration of Zn^{2+}–cyclen derivatives, which may result from the ligand displacement between Fe^{2+} and/or Zn^{2+}.

2. Effects of Zn^{2+}, Cu^{2+}, and Ni^{2+} ions on the aromatic cyclen binding to DNA

Zn^{2+} is essential in the interaction of cyclen derivatives with dT.[38-43,47,48,53-55] In the absence of Zn^{2+}, these ligands did not protect the AT-rich regions, as demonstrated by the DNase I footprinting experiment with **12** (50 μM) (see Figure 4). Upon addition of increasing concentration of Zn^{2+}, the protection of the AT-rich regions emerged (vicinity of 48 and 80 on the Watson strand). On the other hand, other divalent metal ions such as Cu^{2+} or Ni^{2+} were not effective at all, although these ions form more stable 1:1 complexes with cyclen than Zn^{2+}.[56-58] Moreover, Zn^{2+} (up to 50 μM) alone did not protect DNA from the DNase I hydrolysis. These observations are compatible with our prediction based on the T-binding by the Zn^{2+}–cyclen derivatives. We observed that Cu^{2+}– and Ni^{2+}–cyclen derivatives did not interact with dT in the physiological pH.

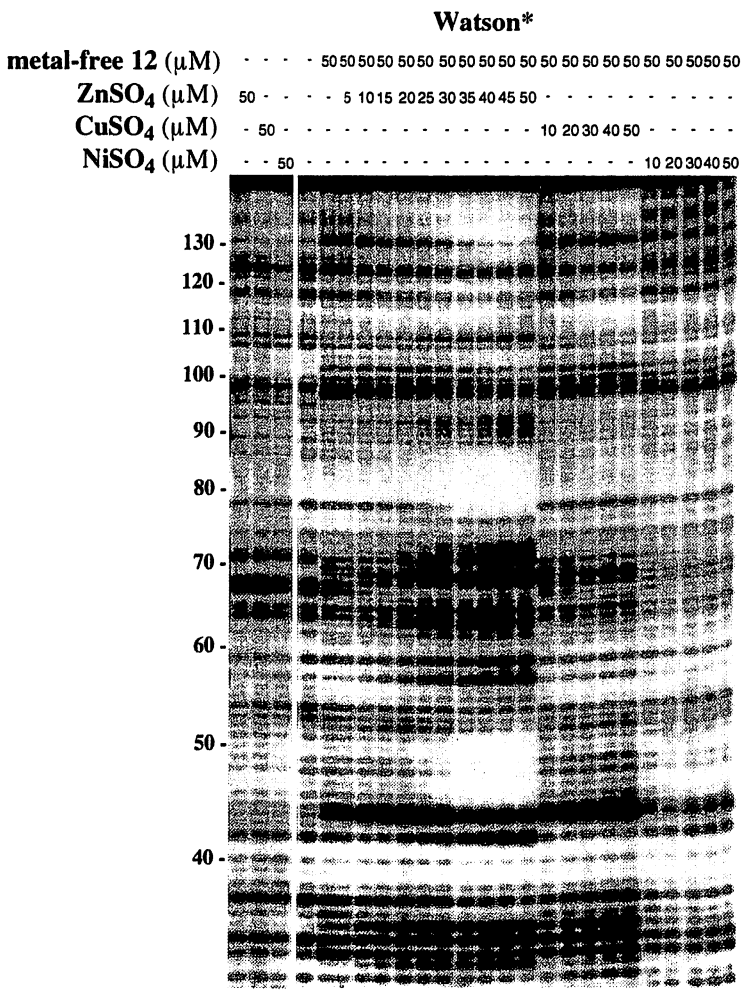

Figure 4 Effect of Zn^{2+} (0 – 50 μM), Cu^{2+} (0 – 50 μM), and Ni^{2+} (0 – 50 μM) on binding of metal-free ligand of **12** (50 μM) to DNA (5'-^{32}P labeled Watson strand).

3. Inhibition of the DNA binding of aromatic Zn^{2+}–cyclen derivatives by thiolate anion (captopril)

A thiolate anion strongly binds to Zn^{2+}–cyclen at the fifth coordination site, as exemplified by captopril complexation (see **16**) with log K of 7.0 at 25°C (i.e., log K_{app} = 4.7 at pH 8).[59] When captopril was added to 50 μM of **12**, the protection of AT-rich regions by **12** was dose-dependently decreased (see Figure 5). This implies that the fifth coordination site of the Zn^{2+}–cyclen should be available for the effective binding with the double-stranded DNA.

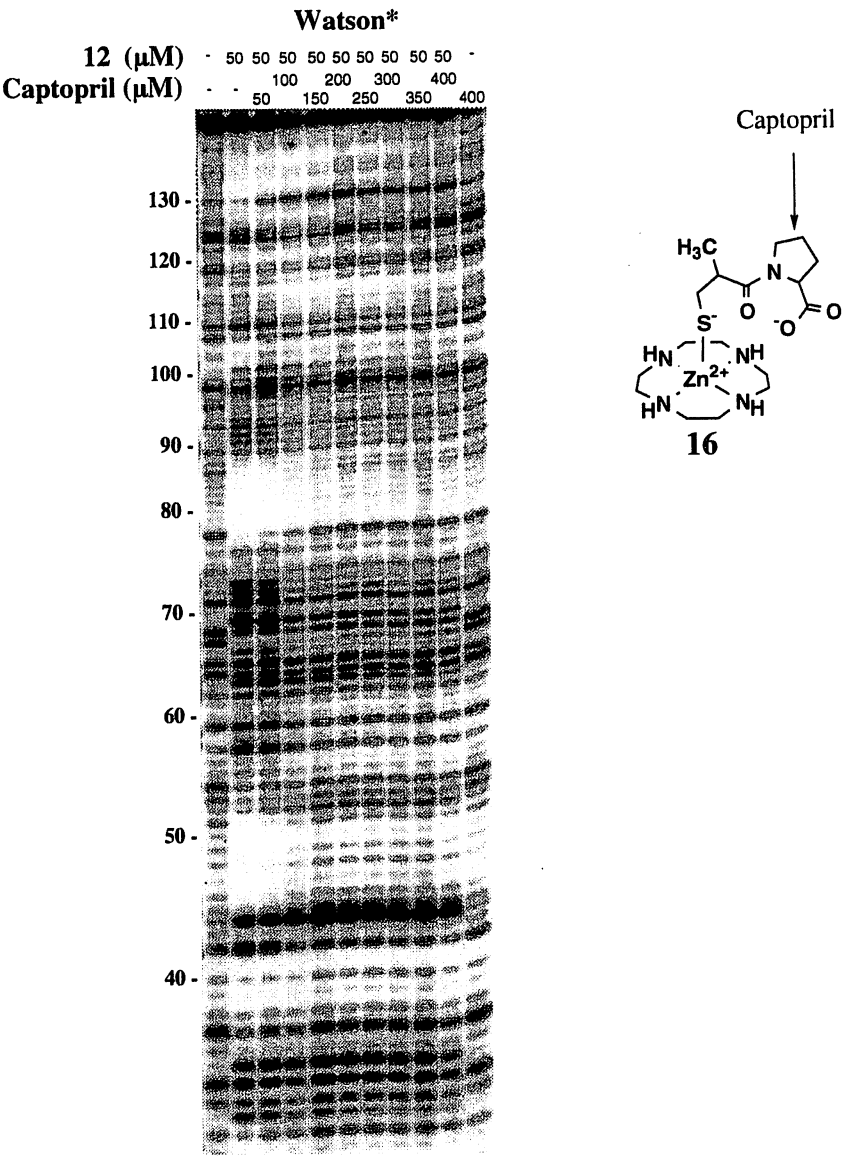

Figure 5 Effect of a thiolate anion, captopril (0 – 400 μM) on **12** (50 μM) binding to DNA (5'-^{32}P labeled Watson strand).

4. Selective recognition of thymine base in DNA by aromatic Zn^{2+}–cyclen derivatives

In order to more precisely characterize the AT-region protected by the Zn^{2+}–cyclen derivatives, we have studied the DNA footprinting by micrococcal nuclease, an enzyme that cuts DNA more efficiently at pA and pT bonds than at pG and pC bonds.[11,45-46] Micrococcal nuclease is known to recognize single-stranded sites in the DNA without too much interference from the opposing strand.[46] This enzyme thus might be extremely useful for comparing the AT recognition mode of the Zn^{2+}–cyclen derivatives with those of distamycin A (**1**) and DAPI (**2**).

Indeed, the micrococcal nuclease footprinting gave a more insightful picture (see Figure 6) than the above DNase I footprinting (see Figure 1) about the interaction of Zn^{2+}–cyclen derivatives with the AT sites. Thus, *Zn^{2+}–cyclen derivatives **7**, **12**, **13**, **14**, and **15** protected almost all the pT bonds from the micrococcal nuclease hydrolysis. On the other hand, they did not protect the pairing pA bonds, resulting in remarkable hydrolysis, especially at homopolymeric A regions* (e.g., the positions 78 – 83 on the Watson strand, 45 – 50 and 103 – 109 on the Crick strand). These results clearly indicate that **7**, **12**, **13**, **14**, and **15** selectively bind to the thymine groups to melt the A–T base pair and that the separated A partners came subject to the strong digestion by micrococcal nuclease (see Figure 7). The released strand –pApApA– from the homopolymeric AT-regions was extremely vulnerable.

In the first DNase I footprinting (see Figure 1), the T and A partners together were protected in the homopolymeric AT-regions. DNase I tends to cut firm double-stranded region rather than breathing single-stranded region, because it recognizes minor groove of DNA and binds across two strands.[46] Hence, the observed protection of homopolymeric AT-regions may simply tell the perturbation of double helical structure by the Zn^{2+}–cyclen derivatives. The exclusive binding of the Zn^{2+}–cyclen derivatives to T was not concluded from the DNase I footprinting.

For distamycin A (**1**) and DAPI (**2**), the micrococcal nuclease footprinting clearly showed that pT and the pairing pA together in the homopolymeric AT-regions were well protected from hydrolysis (e.g., vicinity of the positions 48, 80 on both strands). This fact well reflects that the minor groove binders simultaneously binds to both A and T in the AT minor groove to stabilize the double helix as depicted in Scheme 1. Moreover, these reagents need three or more

consecutive A-T base pairs to bind.[3-15] By comparison, the Zn^{2+}–cyclen derivatives can recognize all the thymine groups in the AT sites.

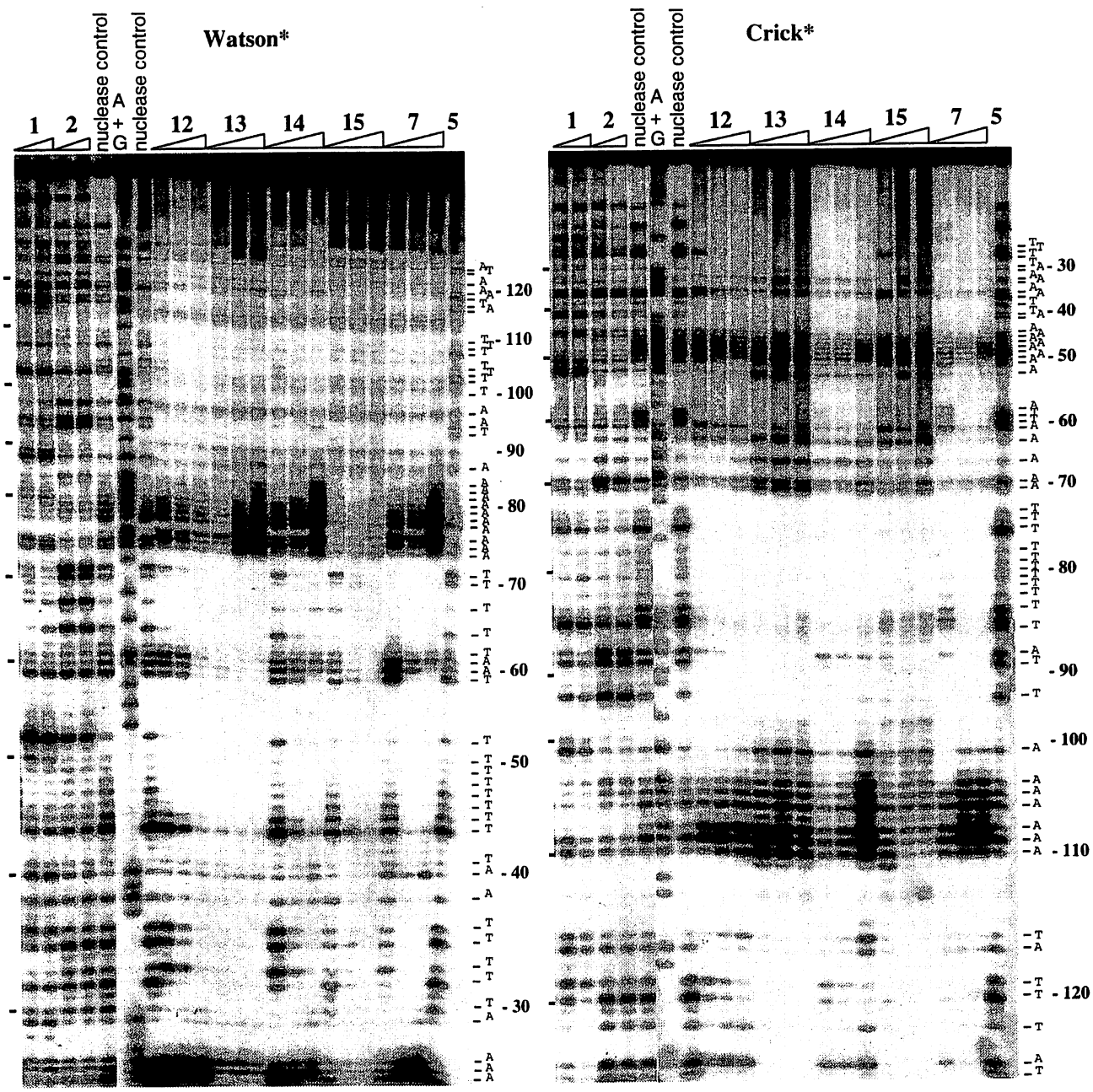

Figure 6 Micrococcal nuclease footprinting in the presence of **1** (5 and 10 μM), **2** (5 and 10 μM), **5** (100 μM), **7** (10, 20, and 30 μM), **12** (40, 60, and 80 μM), **13** (10, 20, and 30 μM), **14** (20, 40, and 60 μM), and **15** (5, 10, and 15 μM). Lane "nuclease control" represents DNA digestion without binders.

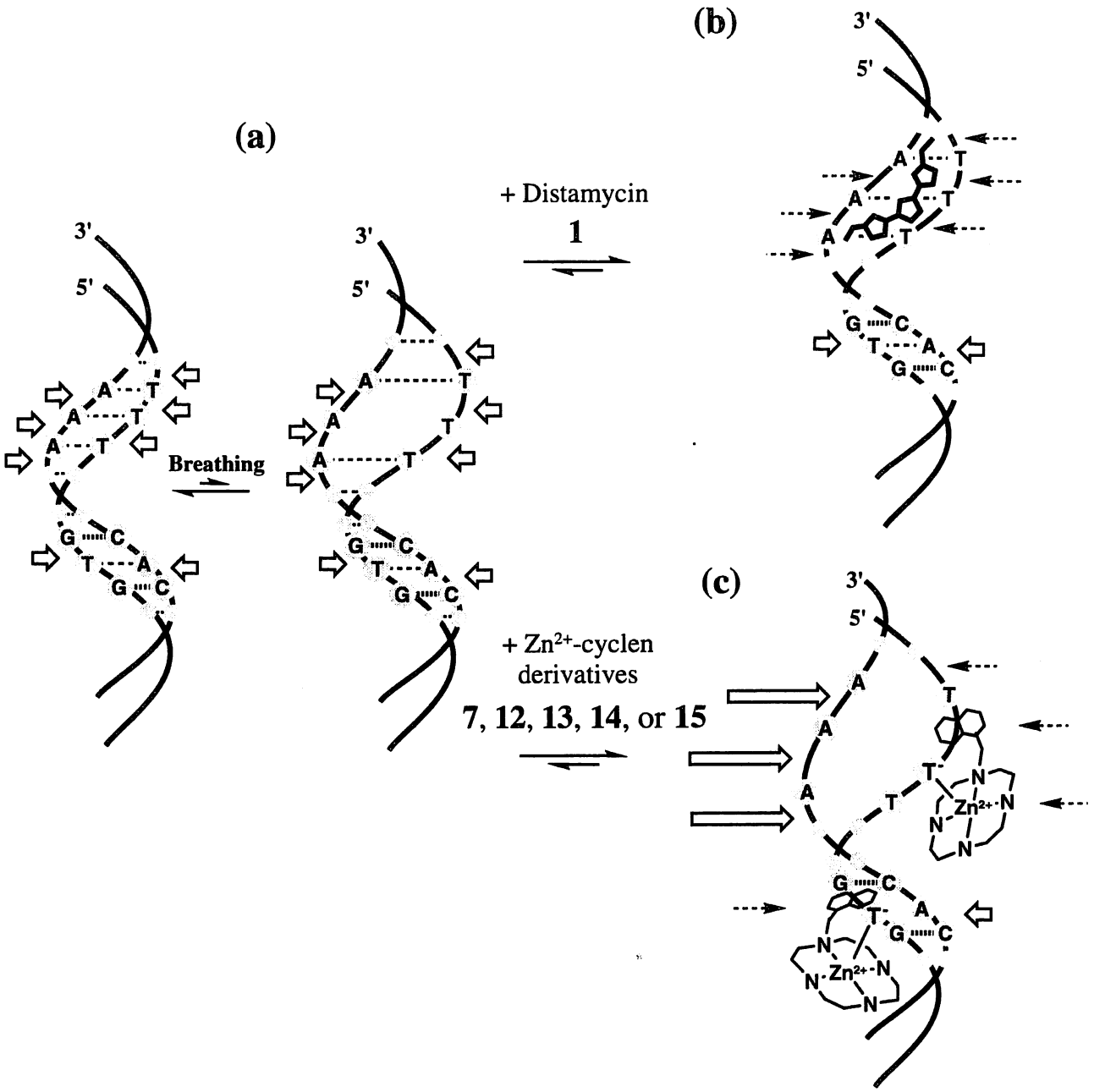

Figure 7 Schematic representation of the micrococcal nuclease attack to (a) breathing double stranded DNA (b) distamycin (**1**)-bound DNA, and (c) Zn^{2+}–cyclen derivative (**7**, **12**, **13**, **14**, or **15**)-bound DNA. Arrows and dashed arrows, respectively, indicate successful and failed hydrolysis by micrococcal nuclease.

5. Competition between distamycin A and aromatic Zn^{2+}–cyclen derivatives for AT-regions in DNA

In order to see that distamycin A (**1**) and **12** share common AT region in equilibrium, a competitive binding study was performed. First, to DNA (5'-^{32}P labeled Watson strand) pre-incubated with 60 μM of **12** was added **1** (0 – 10 μM), which was then digested with micrococcal nuclease (see Figure 8(a)). It was evident that the initial **12**-controlled footprinting pattern at T region (e.g., positions 45 – 50) and A region (e.g., positions 78 – 83) were dose-dependently changed to the **1**-controlled patterns. Conversely, to DNA pre-incubated with 5 μM of **1** was added **12** (0 – 60 μM), which showed that the initial **1**-controlled footprinting patterns were gradually replaced by the **12**-controlled patterns (see Figure 8(b)). Taken these results together, it is concluded that distamycin A and the Zn^{2+}–cyclen complex **12** reversibly compete for common AT regions. The Zn^{2+}–cyclen derivatives would bind to thymine via minor groove of AT region.

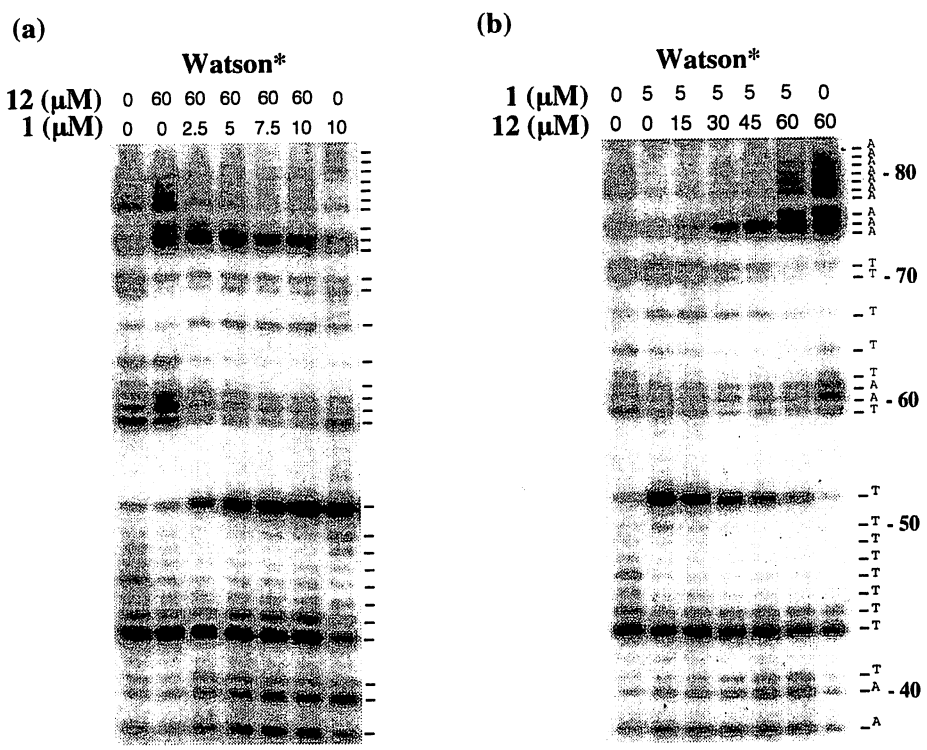

Figure 8 Micrococcal nuclease footprinting assay demonstrating displacement of DNA binding (5'-^{32}P labeled Watson strand): (a) 60 μM **12** by 0 – 10 μM distamycin A (**1**), (b) 5 μM distamycin A (**1**) by 0 – 60 μM **12**.

6. UV and visible absorption spectral changes of the aromatic Zn^{2+}–cyclen derivatives in interaction with calf thymus DNA

The UV and visible absorption spectra of the aromatic pendants of **7**, **12** and **13** changed significantly as a result of their binding to calf thymus DNA. Monitoring such changes would be helpful in estimating the binding constants. In titration of the Zn^{2+}–cyclen derivatives (20 – 40 μM) with DNA (0 – 333 μM) in EPPS buffer (pH 8.0) containing 0.1 M $NaNO_3$ at 25 °C, the absorption maxima of **7** (λ_{max} = 361 nm, ε = 10,030), **12** (λ_{max} = 317 nm, ε = 3,900) and **13** (λ_{max} = 317 nm, ε = 7,400) decreased with an increasing concentration of DNA (hypochromicity) (Figure 9(a) - (c)). Isosbestic points were observed near 310 nm for **7**, 322 nm for **12**, and 320 nm for **13** binding to DNA, suggesting that for each Zn^{2+}–cyclen complex, there is a single mode of binding to DNA. Among these, **7** and **13**, moreover, showed significant red shifts (bathochromism) as [DNA] increased. The bathochromism of **12** was limited in comparison with that of **13**, indicating that the stacking mode of the quinolines was not identical. This fact may result from difference in the single stacking by **12** and double stacking by **13** [in view of significantly higher complexation constants with dT^- (or U^-) and the remarkably different chemical shifts in ^1H NMR data (unpublished), the aromatic rings in **13** are proposed to act as bisintercalators to sandwich thymines]. For comparison, the metal-free ligands of **7**, **12**, and **13** were similarly studied; they showed lesser bathochromisities and smaller hypochromisities than the corresponding Zn^{2+}–cyclen complexes (data not shown).

The changes in the maximum absorbances allowed us to construct the half-reciprocal plots for [DNA] with matching [Zn^{2+}–cyclen derivatives] according to equation (1) in Experimental Section. From the linear half-reciprocal plots for **7**, **12**, and **13** (Figure 9(a') - (c)'), apparent binding constants (K_{app} = [DNA-bound Zn^{2+}–cyclen complexes] / [Zn^{2+}–cyclen complexes][unbound DNA base]) were obtained from the ratio of the slope to the y-intercept (at [DNA] > 100 μM, where the plots gave straight lines; the binding was quantitative[60-61]), which were $3.0 \times 10^4\ M^{-1}$ for **7**, $1.5 \times 10^3\ M^{-1}$ for **12**, and $3.3 \times 10^4\ M^{-1}$ for **13** in 10 mM EPPS buffer (pH 8.0) containing 0.1 M $NaNO_3$ at 25°C. Note that these values were obtained at [DNA] more than five times [Zn^{2+}–cyclen derivatives] (i.e. r = [**7**] / [DNA] < 0.2), where the interaction was derived

mainly from the π-π stacking in the intact double strands, (supplemented by electrostatic forces), but not significantly from the Zn^{2+} - (dT^-) complexation. Similar spectral titrations were conducted for the corresponding metal-free ligands, which gave a smaller K_{app} value of 1.4×10^4 M^{-1} for the metal-free ligand of **7**. The K_{app} values of the metal-free ligands of **12** and **13** couldn't be determined since their hypochromisities were too small to construct the half-reciprocal plot. The K_{app} values for **14** and **15** could not be determined because range of their absorption wavelength (λ_{max} = 283 nm for both **14** and **15**) overlapped with that of calf thymus DNA.

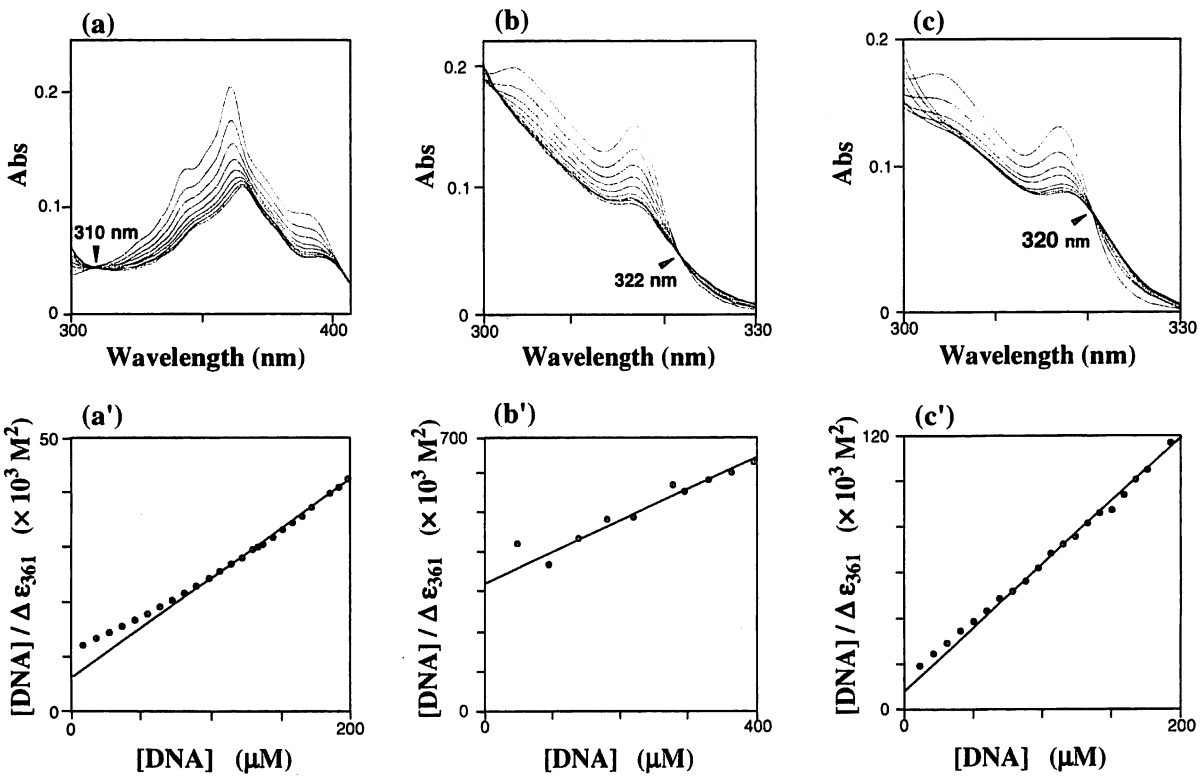

Figure 9 Spectrophotometric titrations of **7** (20 μM) (a), **12** (40 μM) (b), and **13** (25 μM) (c) with calf thymus DNA. The concentrations of DNA phosphates (μM) (r = [Zn^{2+}–cyclen complex] / [DNA phosphates]) are; (a) 0, 29(0.64), 57(0.32), 83(0.21), 107(0.16), 130(0.13), 145(0.11), 167(0.09), and 194(0.08) from the top to bottom curve at 361 nm. (b) 0, 49(1.59), 95(0.82), 140(0.53), 180(0.40), 222(0.32), 281(0.25), 298(0.23), and 333(0.2) μM at 317 nm. (c) 0, 29(0.87), 58(0.43), 86(0.28), 113(0.21), 140(0.17), 165(0.14), and 190(0.12) μM at 317 nm. Arrows indicate isosbestic points. The half-reciprocal plots ([DNA] > 100 μM) for **7**(a'), **12**(b'), and **13**(c').

7. UV and visible absorption spectral changes of Zn^{2+}–acridinylcyclen in interaction with synthetic DNAs

To study further how the Zn^{2+}–cyclen derivatives recognized the specific DNA sequences, the UV and visible absorption spectral changes of **7** were investigated in the presence of synthetic double-stranded DNAs. The spectral changes of 20 μM **7** with poly(dA-dT)$_2$ (0 – 200 μM) in 10 mM EPPS buffer (pH 8.0) containing 0.1 M $NaNO_3$ at 25°C is illustrated in Figure 10(a), which shows one isosbestic point at 310 nm and gives almost a linear half-reciprocal plot (Figure 10(a')). A similar spectral change with one isosbestic point at 310 nm and linear half-reciprocal plots were observed for **7** binding to homo- and hetero- of GC and IC double stranded DNAs (data not shown). From these linear half-reciprocal plots, the K_{app} values were calculated; see Table 3. In the titration of **7** with poly(dA)·poly(dT), mixed equilibria occurred apparently with two different isosbestic points at 340 nm for lower concentration of DNA (< 47 μM) and 290 nm for higher concentration of DNA (> 47 μM) (Figure 10(b)), giving very complex, non-linear half-reciprocal plots (Figure 10(b')). However, if the titration was started with very high [DNA] (> 80 μM) with respect to [**7**] (< 10 μM), the spectral change showed one isosbestic point at 310 nm (Figure 10(c)) and gave a linear half-reciprocal plot (Figure 10(c')) to allow determination of the K_{app} value of 1.1×10^5 M^{-1}.

Without Zn^{2+}, the hypochromism and bathochromism were very limited for any DNA (Table 4). Typical titrations of 20 μM of the metal-free **7** (λ_{max} = 361 nm, ε_{361} = 9,980) with poly(dA-dT)$_2$ (0 – 214 μM) and poly(dA)·poly(dT) (0 – 214 μM) are shown in Figure 10(d) and (e). Similar spectral changes were observed in interaction of the metal-free **7** with other DNAs (data not shown). From the half-reciprocal plots, we have estimated all the K_{app} values for the metal-free **7**, which are all about one order of magnitude smaller than those for the corresponding Zn^{2+}–cyclen complexes (see Table 3).

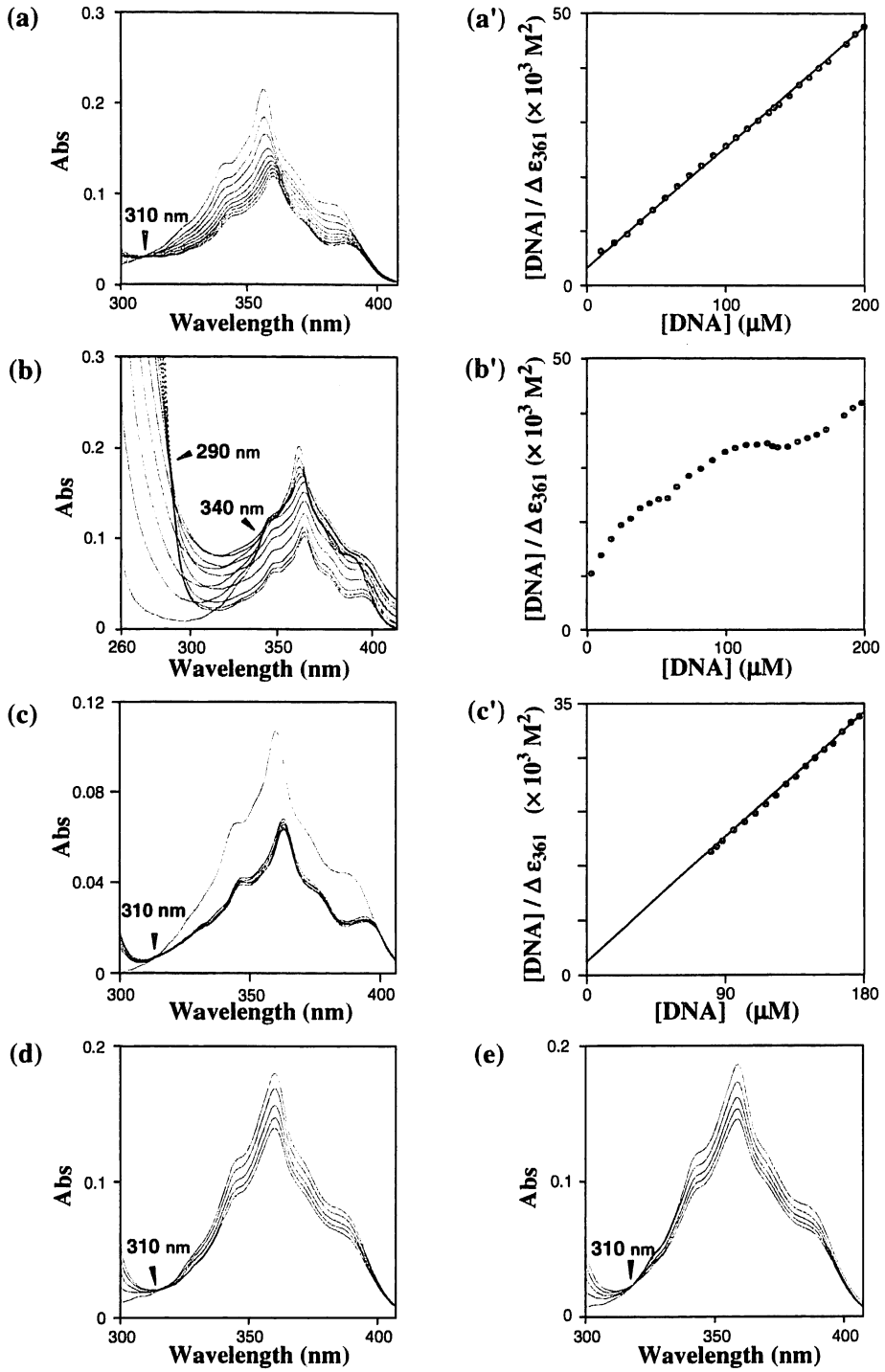

Figure 10 Spectrophotometric titration of **7** (20 μM) with (a) poly(dA-dT)$_2$ or (b) poly(dA)·poly(dT), (c) **7** (10 μM) with poly(dA)·poly(dT), metal-free ligand of **7** (20 μM) with (d) poly(dA-dT)$_2$ or (e) poly(dA)·poly(dT). The concentration of DNA phosphates (μM) (r value) are; (a) 0, 29(0.67), 57(0.33), 83(0.22), 107(0.17), 130(0.13), 145(0.12), 167(0.10), 187(0.09), 200(0.08) from the top to bottom curves at 361 nm. (b) 0, 9(2.15), 19(1.01), 29(0.65), 38(0.49), 47(0.40), 74(0.24), 99(0.18), 122(0.14), 145(0.12), 167(0.10), and 187(0.08) at 361 nm. (c) 0, 80.1(0.11), 101(0.085), 128(0.065), 153(0.052), and 176(0.044) at 361 nm. (d) 0, 58(0.30), 113(0.15), 165(0.10), and 214(0.07) at 361 nm. (e) 0, 58(0.30), 113(0.15), 165(0.10), and 214(0.07) at 361 nm. The half-reciprocal plots for **7** (20 μM) with poly(dA-dT)$_2$ (a') **7** (20 μM) with poly(dA)·poly(dT) (b') **7** (10 μM) with poly(dA)·poly(dT) (c').

Table 3 Apparent binding constants (K_{app} M^{-1}) of **7** and its metal-free ligand with native and synthetic DNAs, as determined by the spectrophotometric titrations in 10 mM EPPS (pH 8.0) containing 0.1 M $NaNO_3$ at 25°C.

DNA	**7**	metal-free **7**	ratio
calf thymus DNA	3.0×10^4 [a]	1.4×10^4 [a]	2.1
poly(dA)·poly(dT)	1.1×10^5 [b]	3.5×10^3 [a]	31.4
poly(dA-dT)$_2$	5.0×10^4 [a]	2.9×10^3 [a]	17.2
poly(dG)·poly(dC)	5.6×10^4 [a]	6.4×10^3 [a]	8.8
poly(dG-dC)$_2$	1.7×10^4 [a]	3.8×10^3 [a]	4.5
poly(dI)·poly(dC)	4.7×10^4 [a]	3.3×10^3 [a]	14.4
poly(dI-dC)$_2$	2.5×10^4 [a]	9.3×10^3 [a]	2.7

[a] By the titration of **7** (20 μM) with DNAs (0 – 220 μM). The half-reciprocal plots were made at [DNA] > 100 μM. [b] By the titration of **7** (10 μM) with poly(dA)·poly(dT) (80 – 180 μM). The half-reciprocal plot was made at [DNA] > 80 μM.

Table 4 Extent of hypochromism (at 361 nm) and red shift (bathochromism).

	Hypochromism(%) [a]		red shift (nm) [b]	
	7	metal-free **7**	**7**	metal-free **7**
calf thymus DNA	54	11	5	ND [c]
poly(dA)·poly(dT)	54	16	5	ND
poly(dA-dT)$_2$	45	5	5	ND
poly(dG)·poly(dC)	61	14	5	ND
poly(dG-dC)$_2$	63	21	5	ND
poly(dI)·poly(dC)	54	13	5	ND
poly(dI-dC)$_2$	45	10	5	ND

[a] Calculated from Δε (equation 1 in experimental section). [b] Calculated from the differences between observed λ_{max} of **7** or metal-free **7** in the absence of DNAs and in the presence of excessive DNAs. [c] Red shift was not detected.

When poly(dA)·poly(dT) (0 - 200 μM) was gradually added to **7** (20 μM), emergence of two isosbestic points suggests that the binding modes differed at lower and higher concentration of DNA (Figure. 10(b)). For comparison, we have measured spectral changes of **7** with each component DNA; i.e. single stranded poly(dA) and poly(dT). The single stranded poly(dA) (Figure 11(a)) showed small hypochromicity with one isosbestic point at 295 nm, and a linear half-reciprocal plot. On the other hand, poly(dT) (Figure 11(b)) showed stronger hypochromism and more remarkable bathochromism, which is somewhat analogous to the initial titration spectra in Figure 10(b). However, the half-reciprocal plots revealed a totally non-linear relation. In this titration of **7** (20 μM) with poly(dA)·poly(dT), [**7**] is initially in large excess, permitting the strong interaction of Zn^{2+}–cyclen moiety with dT to come into play, leading to some disruption of the A-T duplex. However, the spectral titration of **7** (10 μM) with a large excess poly(dA)·poly(dT) (80 – 180 μM) (i.e. $r < 0.11$) (Figure 10(c)) gave a linear half-reciprocal plot (Figure 10(c')), suggesting regular interaction with the intact double strand predominantly by π-π stacking under these conditions. On the other hand, the hetero AT polymer, poly(dA-dT)$_2$, showed only one equilibrium (Figure 10(a)), probably because single strand poly(dA-dT) could maintain the double helical structure by itself, even if the Zn^{2+}–cyclen disrupts the double strand at [**7**] >> [DNA].

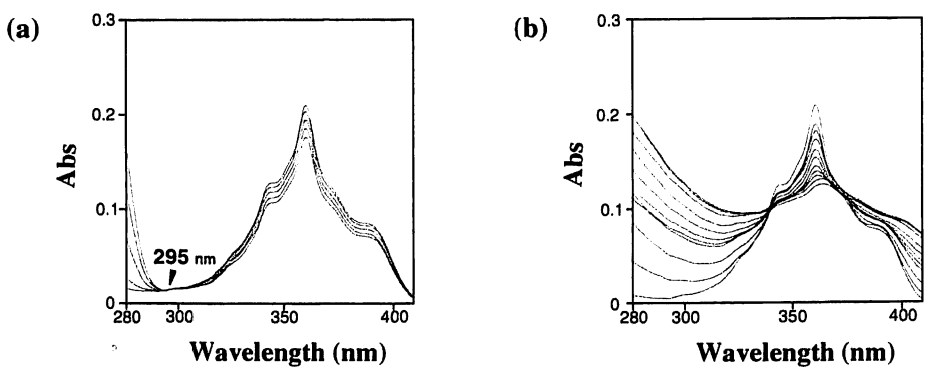

Figure 11 Spectrophotometric titration of **7** with (a) poly(dA) and (b) poly(dT). Initial concentrations of **7** are 20 μM. The concentrations of DNA phosphates (μM) (r) are; (a) 0, 10(1.99), 24(0.81), 41(0.46), and 58(0.31) from the top to bottom curves at 361 nm. (b) 0, 2.0(10.2), 3.8(5.24), 5.7(3.42), 7.0(2.74), 8.3(2.29), 9.5(1.97), 11.5(1.59), 13.8(1.29), 16.0(1.09), and 18.7(0.90) at 361 nm.

In order to know more about the DNA interaction mode of **7**, groove binders and an intercalator displacement experiments were performed (Figure 12(a)). Distamycin (**1**) is known to bind to minor groove at the AT base pairs by hydrogen bonds with adenine N3 and thymine O2.[3-4] The absorbance at 361 nm of **7** decreased upon addition of calf thymus DNA in 10 mM EPPS (pH 8.0) containing 0.1M $NaNO_3$ at 25°C. When the mixing ratio of [**7**] / [DNA phosphates] was [10.5 μM] / [96.0 μM], the ratio of the DNA-bound and DNA-unbound **7** ($[\mathbf{7}_{bound}]$ / $[\mathbf{7}_{free}]$) was calculated to be [8.4 μM] / [2.1 μM] using equation (2) and (3) in Experimental Section. Upon addition of **1**, a decrease was observed in the ratio of $[\mathbf{7}_{bound}]$ / $[\mathbf{7}_{total}]$. The 50% dissociation of the DNA-bound **7** occurred with 6 μM of **1**. Likewise, tested was the displacement by methyl green (**17**), which is known to interact with the hydrophobic surface in the major groove[62] and has AT-specificity.[63] However, in comparison to **1**, **17** did not so significantly promote dissociation of the DNA-bound **7** (50 % dissociation occurred with 30 μM **17**). Ethidium bromide (**18**) was also tested as a non-base selective intercalator. **18** also decreased $[\mathbf{7}_{bound}]$ with an IC_{50} value of 20 μM. Since **1**, **17**, and **18** were reported to possess nearly the same binding affinities to calf thymus DNA (K_{app} = 4 × 10^5 M^{-1} for **1**, 3 × 10^5 M^{-1} for **17**, and 5 × 10^5 M^{-1} for **18** at pH 7.4 and $[Na^+]$ = 0.1 M),[64-65] the outstanding effect by **1** further supports the AT-sequence preference and minor groove specificity of the Zn^{2+}–cyclen derivatives when they interact with calf thymus DNA.

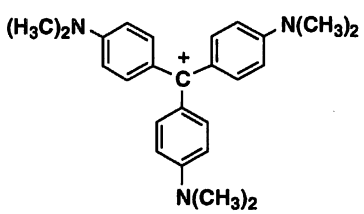

17
Methyl Green

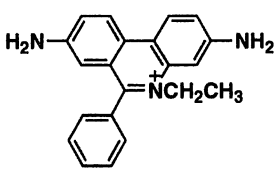

18
Ethidium Bromide

The interaction of the metal-free ligand of **7** with DNA was also blocked, but almost indiscriminately by **1** and **18** (Figure 12(b)). When the mixing ratio of [metal-free **7**] / [DNA phosphates] was [10.1 μM] / [96.0 μM], where the ratio of the [metal-free $\mathbf{7}_{bound}$] / [metal-free $\mathbf{7}_{free}$] was calculated to be [6.4 μM] / [3.7 μM], the 50 % dissociation of the metal-free **7** occurred with the same 1.7 μM of **1** and **18**.

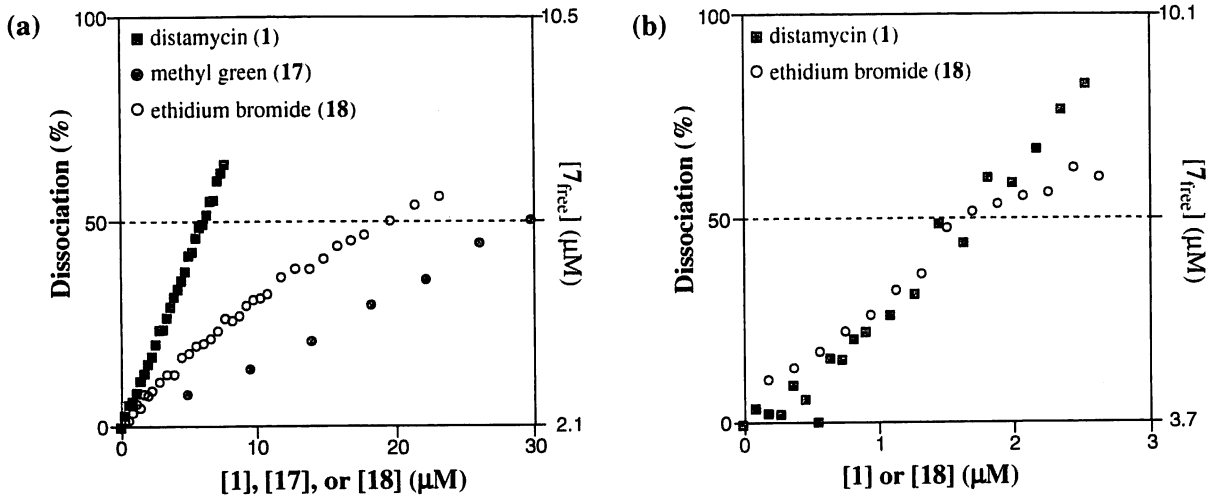

Figure 12 Competition profiles of groove binders (**1** or **17**) and an intercalator (**18**) in DNA binding of (a) **7** and (b) the metal-free **7**. The cross point of middle dashed line indicates 50% dissociation concentration (IC_{50}).

8. DNA Melting by Zn^{2+}–acridinylcyclen

Additional information on the DNA binding properties of the Zn^{2+}–cyclen derivatives were obtained from the DNA melting studies. The DNA (all 50 μM in 10 mM EPPS (pH 8.0 at 25°C) containing 15 mM $NaNO_3$) melting profiles in the presence of increasing concentration of **7** and its metal-free ligand are shown in Figure 13. The melting temperatures (T_m) of poly(dA)·poly(dT) and poly(dA-dT)$_2$ initially increased (ΔT_m = + 4.7°C for poly(dA)·poly(dT) and ΔT_m = + 3.4°C for poly(dA-dT)$_2$ at r = [**7**] / [DNA phosphates] = 0.1 in Figures 13(b) and (c)). However, later T_m began to decrease (e.g. ΔT_m = -3.3°C for poly(dA)·poly(dT) at r = 0.2 and ΔT_m = -1.3°C for poly(dA-dT)$_2$ at r = 0.3). The melting profile of calf thymus DNA (its AT content = 58%) was somewhat similar to that of these AT polymers (Figure 13(a)). On the other hand, the double strands poly(dI)·poly(dC) and poly(dI-dC)$_2$ were steadily stabilized by **7** (Figures 13(d) and (e)). Likewise, the metal-free ligand of **7** steadily stabilized the double strand of calf thymus DNA and all the synthesized DNAs (Figures 13(a') - (e')).

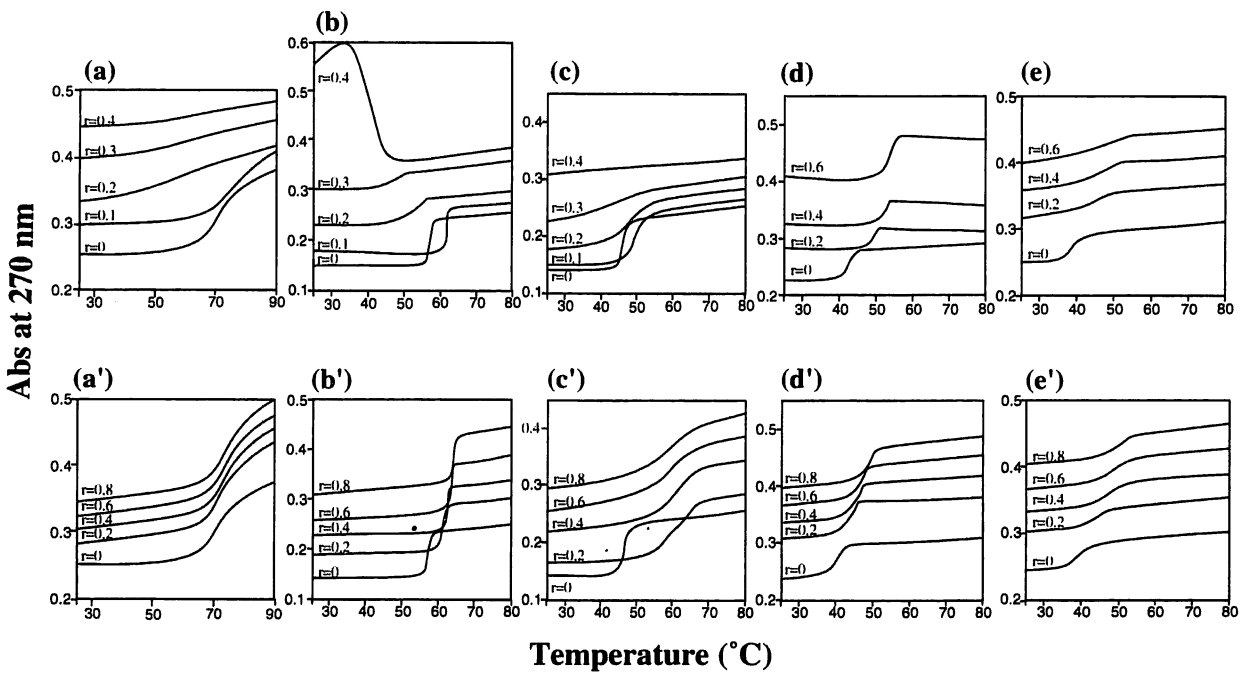

Figure 13 Native and synthetic DNAs (all 50 μM in 10 mM EPPS (pH 8.0 at 25°C) containing 15 mM $NaNO_3$) melting profiles in the presence of (a)-(e) **7** or (a')-(e') metal-free **7**. (a)(a') Calf thymus DNA, (b)(b') poly(dA)·poly(dT), (c)(c') poly(dA-dT)$_2$, (d)(d') poly(dI)·poly(dC), and (e)(e') poly(dI-dC)$_2$.

II Controlling gene expression by zinc(II)–macrocyclic tetraamine complexes

1. Inhibition of *in vitro* transcription of *E. coli* RNA polymerase by aromatic Zn^{2+}–cyclen derivatives

To test if the interaction of the Zn^{2+}–cyclen complexes with DNA affects some biochemical processes, Zn^{2+}–cyclen complexes **5**, **7**, **12**, **13**, **14**, **15**, and their metal-free ligands were examined for their ability to inhibit *in vitro* transcription from calf thymus DNA (250 μM) as a template by *E. coli* RNA polymerase. The calf thymus DNA-directed transcription was assayed by measuring the incorporation of [^{3}H]-UTP using the same method applied to the actinomycin D transcriptional inhibition test.[23] Reactants also contained all other nucleotide substrates (each 200 μM) needed for RNA synthesis. Indeed, the inhibition of the transcription took place with the Zn^{2+}–cyclen complexes **7**, **13**, and **14**, but not with the metal-free ligands. The 50 % inhibition concentrations (IC_{50}) of the Zn^{2+}–cyclen complexes are summarized in Table 5. The most effective complex was the Zn^{2+}–bisnaphthylcyclen **15**.

Then, we tested **7** to inhibit the transcription from the synthetic DNAs; i.e. with poly(dA-dT)$_2$, poly(dA)·poly(dT), and poly(dG-dC)$_2$ (all 20 μM) as templates. The inhibition profiles are shown in Figure 14. For the poly(dA-dT)$_2$ template, incorporation of either [^{3}H]-ATP or [^{3}H]-UTP substrate was inhibited to the same degree with IC_{50} = 36 μM and 33 μM, respectively (Figure 14 (a)). On the other hand, for the poly(dA)·poly(dT) template the incorporation of [^{3}H]-ATP (IC_{50} = 22 μM) was not the same as of [^{3}H]-UTP (IC_{50} = 45 μM), the former being more effectively blocked (Figure 14(b)). This fact is compatible with the prediction that **7** strongly binds to poly(dT) strand. For the poly(dG-dC)$_2$ template, the incorporation of [α-^{32}P]-CTP was weakly inhibited (IC_{50} = 110 μM), implying that in the transcription this template was not as effectively blocked as the AT polymers by **7** (Figure 14(c)).

Table 5 The 50% inhibition (IC_{50}) of calf thymus DNA (250 μM)-directed transcription by Zn^{2+}–cyclen derivatives or its metal-free ligand.

	IC_{50} (μM)	
	Zn^{2+}–complex	metal-free ligand
5	> 200	>200
7	130	>200
12	> 200	>200
13	95	> 200
14	> 200	> 200
15	55	>200

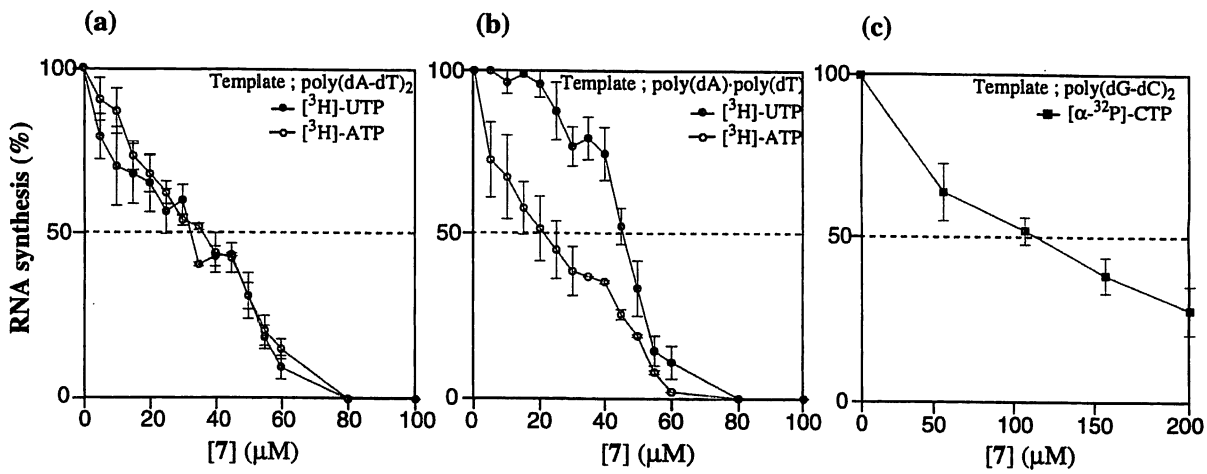

Figure 14 Inhibition profiles of *in vitro* transcription using *E. coli* RNA polymerase by **7**. (a) [^{3}H]-ATP or [^{3}H]-UTP incorporation directed by poly(dA-dT)$_2$, (b) [^{3}H]-ATP or [^{3}H]-UTP incorporation directed by poly(dA)·poly(dT), and (c) [α-^{32}P]-CTP incorporation directed by poly(dG-dC)$_2$.

2. Inhibition of topoisomerases by aromatic Zn^{2+}–cyclen derivatives

Type I and type II topoisomerases are nuclear enzymes that catalyze the relaxation of negative supercoils and the stepwise negative supercoiling of DNA, respectively, in many cellular processes such as replication and transcription.[67] The minor groove binders (**1** and **2**) prevent the topoisomerase activities at μM concentrations.[68-71] In order to see the effect of the Zn^{2+}–cyclen derivatives on the topoisomerase reactions, we now have conducted topoisomerase inhibition experiments using form I pBR322 DNA (see Figure 15, commercial pBR322 contains impurity form II).

In the absence of the inhibitory agents, type I topoisomerase converts the form I (supercoiled) pBR322 into several relaxed forms, (see the run at [**15**] = 0 μM). In the presence of increasing concentration of the Zn^{2+}–bisnaphthylcyclen **15**, the formation of the relaxed forms of pBR322 was reduced and the greater ratio of the form I remained unchanged (see Figure 15). The concentration for 50% inhibition (IC_{50}) of catalytic activities of type I topoisomerase, defined as the drug concentrations to keep the 50 % remain of the original form I pBR322, was ca. 200 μM, which represents ca. three times weaker activity than those of **1** (IC_{50} = 70 μM) and **2** (60 μM). Although other zinc(II) complexes such as **7**, **12**, **13**, and **14** showed smaller (but definite) inhibition activities in the type I topoisomerase reaction, we could not determine quantitative values of IC_{50} under the same conditions (see experimental section).

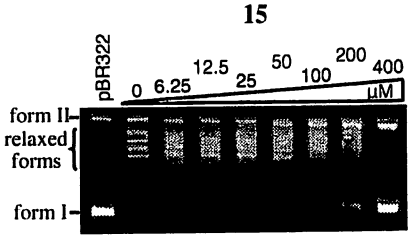

Figure 15 The effect of **15** (0 – 400 μM) on relaxation of form I pBR322 DNA by type I topoisomerase.

Next, we examined whether type II topoisomerase reaction was affected by the Zn^{2+}–cyclen derivatives. Indeed, similar dose-dependent inhibition was observed for the zinc(II) complexes **7**, **12**, **13**, **14**, and **15** (see Figure 16). Among those zinc(II) complexes, **15** was the most effective inhibitor (see Table 6), whose activity (IC_{50} = 10 μM) was greater than those of **1** (40 μM) and **2** (30 μM). The metal-free ligands were much weaker inhibitors (i.e., IC_{50} > 400 μM for the ligands of **7**, **12**, **13**, and **14** and ca. 100 μM for the ligand of **15**) than the corresponding zinc(II) complexes. Thus, zinc(II) ion in the cyclen macrocycle also acts a major role in the type II topoisomerase inhibition.

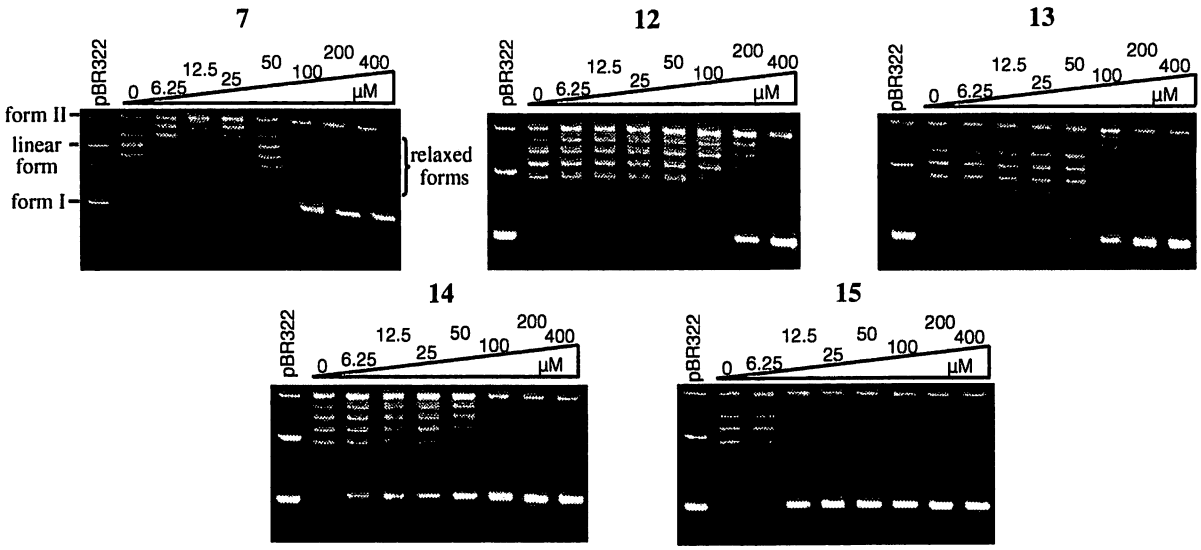

Figure 16 The effects of **7**, **12**, **13**, **14**, and **15** (0 – 400 μM) on relaxation of form I pBR322 DNA by type II topoisomerase.

Table 6 Concentrations for 50% inhibition (IC_{50})[a] of the type II topoisomerase.

	IC_{50} (μM)
7	70
12	250
13	100
14	40
15	10
1	40
2	30

[a] IC_{50} values were defined as the concentrations required for 50 % remain of the form I pBR322 in the catalytic reaction of the type II topoisomerase. The estimated error in the IC_{50} values was ± 20%.

3. Antimicrobial activities of aromatic Zn^{2+}–cyclen derivatives

The antimicrobial activities against a gram-positive bacteria (*Staphylococcus aureus* FDA209P) and a gram-negative bacteria (*Escherichia coli* NIHJ) were tested by a microtiter plate method for the Zn^{2+}–cyclen derivatives and corresponding metal-free ligands, along with **1** and **2**. The obtained minimum inhibitory concentrations (MIC) are listed in Table 7. For comparison, **2**, which is often used as a fluorescent chromosome stain in cytochemical studies[66] showed strong antimicrobial activity aginst both bacterial strains (MIC = 0.4 μM for *S. aureus* and 0.8 μM for *E. coli*). An antiviral antibiotic **1**, is not so effective against both strains.

The Zn^{2+}–complexes of **7**, **13**, and **15** showed strong antimicrobial activities against *S. aureus*, which is compatible to the DNase I footprinting titration results showing higher affinity of **7**, **13**, and **15** with DNA than **12** and **14**. On the other hand, their metal-free ligands were not effective at all (up to 50 μM). These antimicrobial behaviors may suggest that the zinc(II) complexes having hydrophobic aromatic rings probably permeate into the hydrophobic membrane of gram-positive bacteria (but could not permeate the hydrophilic component-containing gram-negative bacterial membrane) to inhibit the bacterial growth by the strong DNA binding.

Table 7 Minimum inhibitory concentrations (MICs, μM) against *S.aureus* FDA 209P and *E. coli* NIHJ.

	S.aureus FDA209P		*E.coli* NIHJ	
	Zn^{2+}–complex	metal-free ligand	Zn^{2+}–complex	metal-free ligand
5	>50	>50	>50	>50
7	13	>50	>50	>50
12	>50	>50	>50	>50
13	25	>50	>50	>50
14	50	>50	>50	>50
15	1.7	6.3	6.3	6.3
1	25		50	
2	0.4		0.8	

4. Interaction of aromatic Zn^{2+}–cyclen derivatives with TATA box in SV 40 early promoter

The AT-rich DNA sequence located 25 to 30 bp upstream from the transcriptional start sites (so-called TATA box) is known as an essential element of the promoter for eukaryotic RNA polymerase II.[72] The TATA box plays a key role in regulating the overall level of transcription and participates in selecting the transcriptional start site, where some transcriptional factors (e.g., TATA binding protein (TBP)) bind for initiation of the transcription.[73] The minor groove binders, distamycin A (**1**) and DAPI (**2**) are known to strongly bind to the TATA box and thus inhibit the binding of TBP.[74-75]

In order to evaluate the binding of the Zn^{2+}–cyclen derivatives (**7**, **12**, **13**, **14**, and **15**) to the TATA box, we have conducted a DNase I footprinting experiment with a 197-bp SV40 early promoter sequences containing AT-rich TATA box (TATTTAT) and GC-rich GC boxes (Figure 17(a)). The result confirmed that the Zn^{2+}–cyclen derivatives indeed showed stronger binding to the TATA box than to any other region (see Figure 17(b)).

Next, the inhibitory effect of the Zn^{2+}–cyclen derivatives on the binding of human TBP to TATA box was determined by a gel mobility shift assay with a 25-bp TATA consensus DNA fragment (see experimental section). Typical photographs for the gel mobility shift assay in the absence and presence of **7**, **12**, **13**, **14**, or **15** are shown in Figure 18. With an increase in the concentration of Zn^{2+}–cyclen derivatives, the concentration of the TBP-DNA complex was reduced. The metal-free ligands, however, demonstrated no effect on the TBP binding to DNA (see far light end, Figure 18). These facts showed that the TBP–DNA formation was inhibited by those Zn^{2+}–cyclen derivatives and zinc(II) ion was essential for the inhibition. Concentrations of 50% inhibition (IC_{50}) in the TBP–DNA formation by the Zn^{2+}–cyclen derivatives and the minor groove binders (**1** and **2**) are summarized in Table 8. Although the Zn^{2+}–cyclen derivatives were not so powerful inhibitors (e.g., IC_{50} = 2.5 μM for **13**) in comparison to **1** (IC_{50} = 0.4 μM) and **2** (0.8 μM), those biological activities indicate that Zn^{2+}–cyclen derivatives are a new promising prototype as a small molecular genetic transcriptional regulation factor.

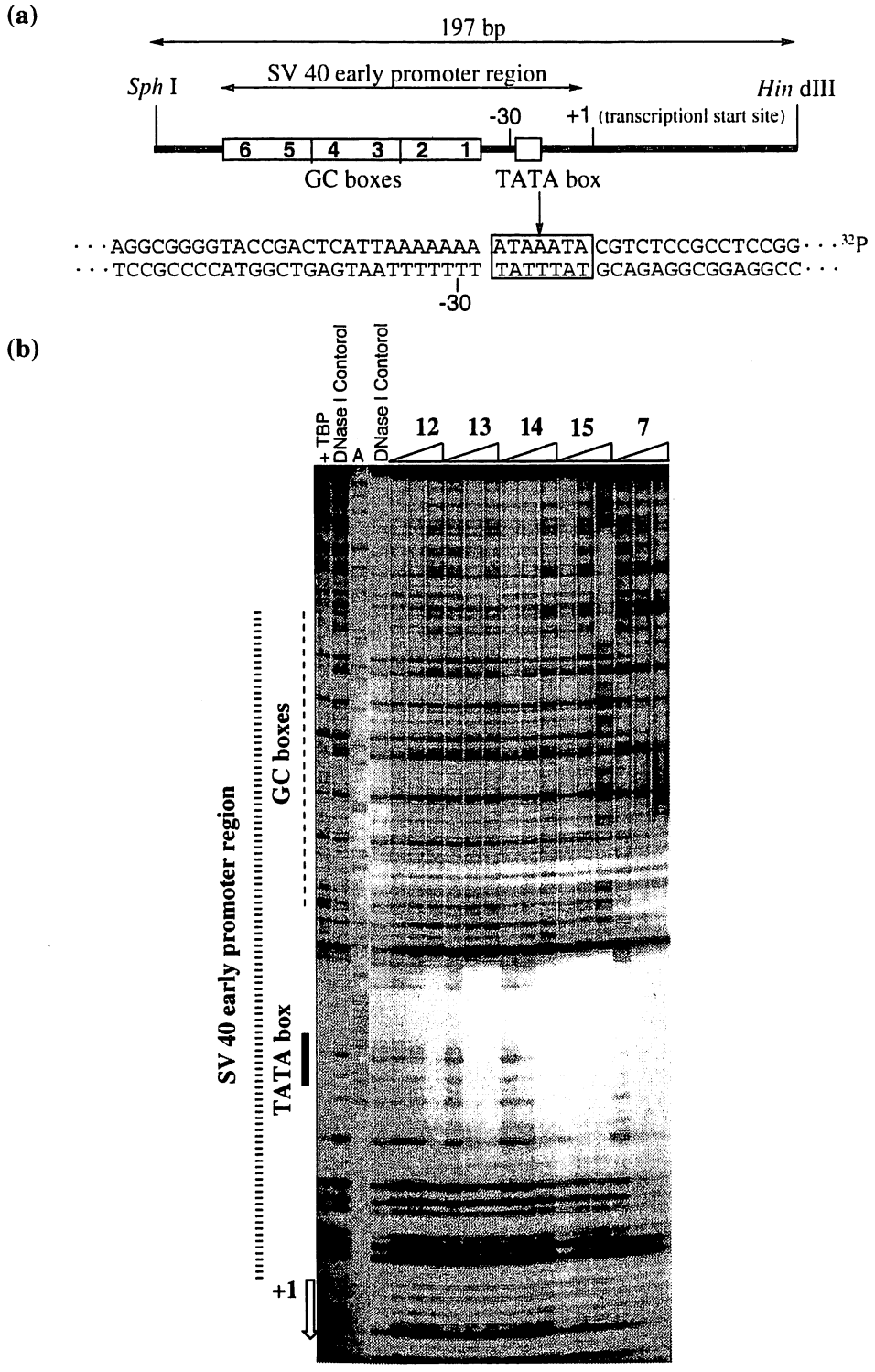

Figure 17 (a) Schematic representation of the SV40 early gene promoter region DNA (197 bp) used in the DNase I footprinting assay. The DNA sequence of the TATA box region is shown. (b) DNase I footprinting of 197-bp SV40 early gene promoter DNA in the presence of **12** (25, 50, and 100 μM), **13** (3.13, 6.25, and 12.5 μM), **14** (25, 50, and 100 μM), **15** (1.56, 3.13, and 6.25 μM), and **7** (6.25, 12.5, and 25 μM). The lane "A" represents the dideoxy sequencing marker specific for adenine. The lane "DNase I control" and "TBP" represents DNA digested with DNase I without binders and with TBP, respectively.

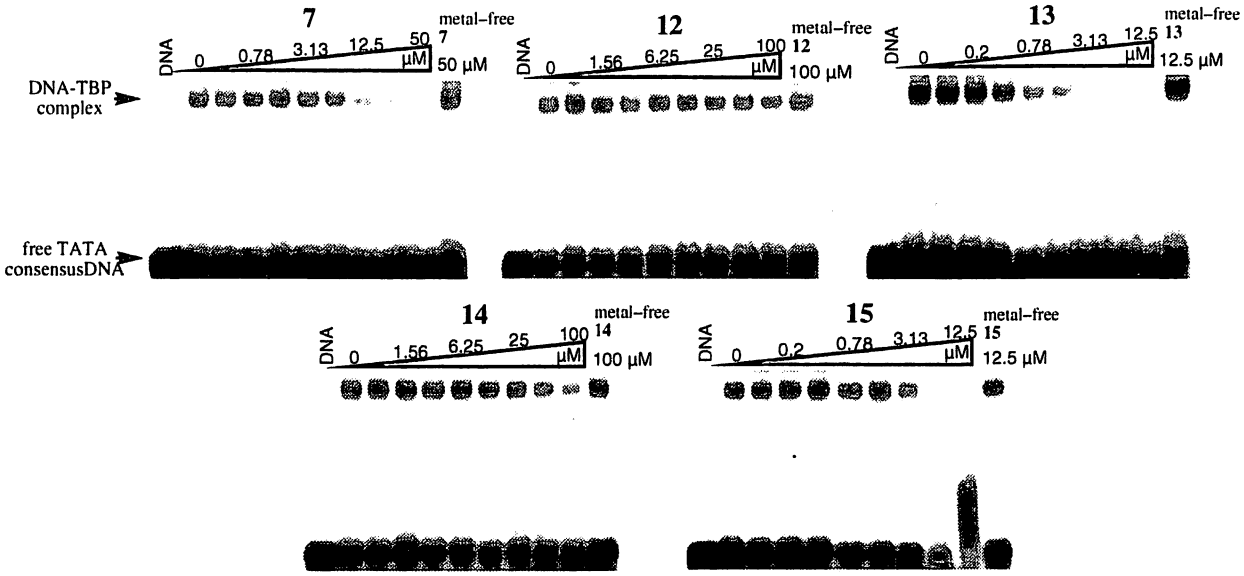

Figure 18 Gel mobility shift assay for a TATA box consensus DNA fragment in the presence of TBP, showing the titration with increasing amounts of cyclen derivatives **7** (0 – 50 μM), **12** (0 – 100 μM), **13** (0 – 12.5 μM), **14** (0 – 100 μM),and **15** (0 – 12.5 μM). Lane "DNA" represents DNA without TBP.

Table 8 Concentrations of 50% inhibition (IC_{50}) of TBP-DNA complex formation.

	IC_{50} (μM)
7	15
12	70
13	2.5
14	>100
15	4
1	0.4
2	0.8

5. Selective recognition of consecutive G sequence in double-stranded DNA by Zn^{2+}–anthraquinonylcyclen

We now have found that Zn^{2+}–(2-anthraquinonyl)methyl-cyclen (= Zn^{2+}–anthraquinonylcyclen (**19**)), which originally was designed as a redox-active sensor for selective dT (or U) nucleoside in aqueous solution,[47] more favorably *binds to guanine- than thymine-rich sequence in double-stranded DNA.* While the preference of nucleobase dT over dG was more or less similar by **19**[47] (K_d values for complexation of **19** with dT, and dG at pH 8 were 79 μM and 1 mM, respectively), and the Zn^{2+}–acridinylcyclen **7**, their affinities to nucleobases in double stranded DNA seemed completely different: **19** favored G-rich DNA, while **7** favored T-rich DNA.

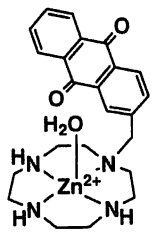

19

Zn^{2+}–(2-anthraquinonyl)-methyl-cycler

In literature,[76-84] a number of anthraquinone derivatives (including antibiotics such as prospermine[77] daunomycin,[81-82] and mitoxanthrone[84]) have been shown to interact with G-rich sequences as intercalators or groove binders and cleave GpG strands photochemically,[78-81] or to inhibit telomerase.[82-83] The features of **19** as a new prototype of selective G-binding agent are described herein, in comparison to those for the T-recognizing **7** and the conventional GC-recognizing actinomycin **4**.

The UV absorption spectra of the anthraquinone moiety of the metal-free ligand **19** (which is in a diprotonated form, $L{\cdot}2H^+$ at pH 8.0), the Zn^{2+}–complex **19**, and Cu^{2+}–complex **19** changed more significantly (stronger hypochromisms and bathochromisms) in their binding to double stranded DNA's (e.g., poly(dG)·poly(dC)). Monitoring such changes would permit estimation of the binding constants.[60-61] In a typical titration, poly(dG)·poly(dC) (0 – 200 μM nucleobase in DNA) was added to **19** (20 μM) in EPPS buffer (pH 8.0) with I = 0.1 ($NaNO_3$) at

25°C (Fig. 19). For comparison, the metal-free **19** (λ_{max} = 334 nm, ε_{334} = 5,420), its Cu^{2+}–complex **19** (λ_{max} 334 nm, ε_{334} = 6,330), and actinomycin D **4** were similarly studied.

The smooth decreases in the maximum absorbance allowed us to construct half-reciprocal plots for [nucleobase in DNA] with [**19**] according to equation 1 (see Experimental Section) derived earlier,[60-61] as done with **7**. Isosbestic points were observed in the titration with poly(dG)·poly(dC) (see Figure 19(a)–(c)), suggesting each single mode of **19**, metal-free **19**, and Cu^{2+}-complex **19** binding to DNA. From the linear half reciprocal plots (Figure 19(a')–(c')), apparent binding constants, K_{app} were determined at [nucleobase in DNA] > 100 μM, where the plots gave straight lines.[60-61] Calf thymus and other synthetic DNA's gave similar titration behaviors, except for poly(dA)·poly(dT), where irregular spectrophotometric titration (Figure 19(d)-(e)) and the non-linear half-reciprocal plots were seen. All the K_{app} values thus determined are summarized in Table 9, along with the corresponding values with **7**.

Table 9 Comparison of apparent binding constants, K_{app} (M^{-1})[a] of anthraquinonylcyclen derivatives **19**, acridinylcyclen derivatives **7**, ethidium bromide **18**, and actinomycin D **4** with native and synthetic DNAs, as determined by the spectrophotometric titration in 10 mM EPPS (pH 8.0) with I = 0.1 M ($NaNO_3$) at 25°C.

	$K_{app} \times 10^{-4}$							
	Metal-free		Cu^{2+}–complex	Metal-free		Cu^{2+}–complex		
DNA	**19**	**19**	**19**	**7**	**7**	**7**	**18**	**4**
calf thymus DNA	0.59	2.8	0.89	1.4[b]	3.0[b]	1.2	1.1	0.71
poly(dG)·poly(dC)	0.53	15	12	0.64[b]	5.6[b]	8.5	3.8	2.9
poly(dG-dC)$_2$	0.74	2.8	1.1	0.38[b]	1.7[b]	–[d]	4.5	13
poly(dA)·poly(dT)	-[c]	-[c]	0.56	0.35[b]	11[b]	0.03	0.65	–[d]
poly(dA-dT)$_2$	0.74	4.3	2.7	0.29[b]	5.0[b]	–[d]	1.7	–[d]

[a] K_{app} = [DNA-bound **7**, **19**, **18**, or **4**]/[uncomplexed**7**, **19**, **18**, or **4**][uncomplexed nucleobase in DNA] (M^{-1}). The estimated errors in the K_{app} values were ±10%. [b] data from table 3. [c] K_{app} values could not be determined due to irregular spectral changes, see text. [d] Not determined.

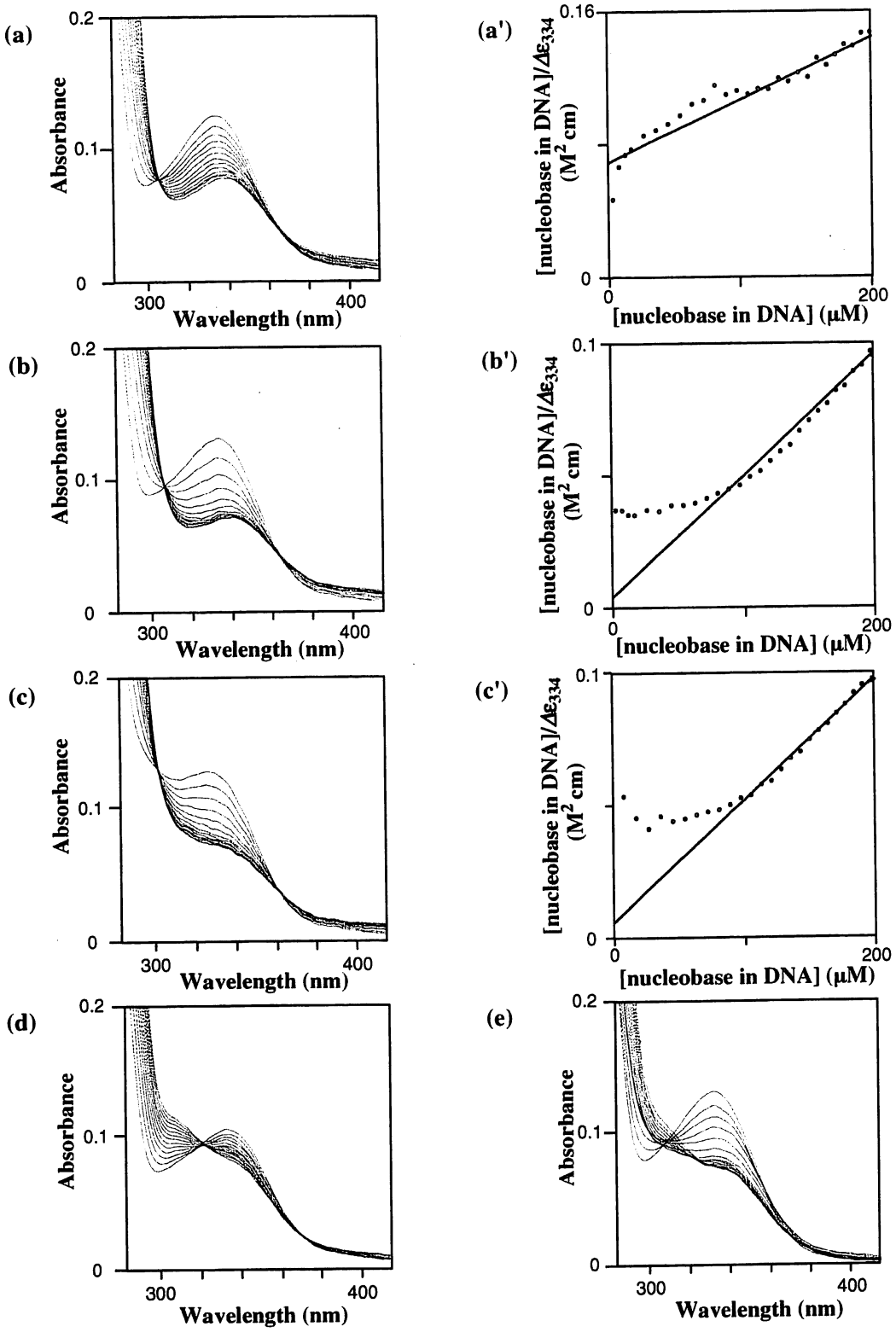

Figure 19 UV spectrophotometric titrations: (a) for metal-free **19**, (b) for **19**, and (c) for Cu^{2+}–complex **19** (each 20 μM) with poly(dG)·poly(dC) (0 – 200 μM from top to bottom curves at 334 nm); their half-reciprocal plots (a'), (b'), and (c'), respectively. (d) for metal-free **19** and (e) for Cu^{2+}–complex **19** (each 20 μM) with poly(dA)·poly(dT)(0 - 200 μM from top to bottom curves at 334 nm).

The metal-free **19** (as diprotonated cation at pH 8.0) interacted with all the measured DNA's with more or less the same affinities of an order of 3 – 4, indicating the π-π stacking as the major common interaction. In separate experiments, metal-free **19** did not interact with all the nucleosides. The Zn^{2+}–complex **19** generally showed higher affinity than the metal-free **19** or the Cu^{2+}–complex **19**. Among the measured DNA's, poly(dG)·poly(dC) had the highest affinity with **19** (K_{app} = 1.5 × 10^5 M^{-1}), whereas poly(dG-dC)$_2$ did not so strongly bind to **19** (K_{app} = 2.8 × 10^4 M^{-1}). This is to be compared with the preference of poly(dG-dC)$_2$ (K_{app} = 1.3 × 10^5 M^{-1}) to poly(dG)·poly(dC) (K_{app} = 2.9 × 10^4 M^{-1}) by the GpC-recognizing actinomycin D **4**.[20-23]

We independently measured the DNA binding of the GC-recognizing agents **4** by the displacement assay of the DNA-stacked fluorescence dye ethidium bromide (**18**).[85-86] The stacking of **18** (λ_{max} = 480 nm, ε_{480} = 5,580) with various DNA's was measured by the identical UV spectrophotometric titrations used for **7**, **19**, and **4** in 10 mM EPPS buffer (pH 8.0) with I = 0.1 ($NaNO_3$) at 25 °C. The results (Table 9) showed that, although **18** has a little GC preference, it binds to DNA's with a similar order of affinities (K_{app} = ~ 10^4 M^{-1}). These results are in agreement with the reported DNA binding affinity and sequence preference of **18**.[78,87] It is to be added that **18** showed almost the same affinity to homopolymeric poly(dG)·poly(dC) (K_{app} = 4.5 × 10^4 M^{-1}) and heteropolymeric poly(dG-dC)$_2$ (K_{app} = 3.8 × 10^4 M^{-1}).

The easiness of displacing DNA-bound ethidium bromide is a qualitative measurement of the DNA affinity.[85-86] With all the DNA's, the addition of **19** or **4** caused smooth decreases in the fluorescence emitted from the DNA-bound **18**, indicating the smooth displacement of **18** by **19** or **4**. The C_{50} values were determined as the concentration of **19** required for a 50% reduction of the fluorescence (excitation at 520 nm, emission at 600 nm) with [**18**] or [**4**] = [nucleobase in DNA] = 2 μM in the buffers. It would be reasonable to assume that the smaller is the C_{50} value, the stronger is the interaction to drive off **18** from the same DNA. The results summarized in Table 10 showed that the Zn^{2+}–complex **19** is far more efficient (i.e. smaller C_{50} values) than the metal-free **19** in displacing the stacked ethidium bromide in any DNA, lending a support to the stronger binding (K_{app} values) of **19** than of metal-free **19** obtained by the independent UV spectrophotometric titrations (Table 9). **19** showed the smaller C_{50} value (= 0.4 μM) for poly(dG)·poly(dC) than 2.0 μM for poly(dG-dC)$_2$, which is somewhat parallel to the binding

constants K_{app}, although these C_{50} and K_{app} values may not be directly correlated. It is of interest to see that the GpC-recognizing **4**[20-23] was more effective in driving off the poly(dG-dC)$_2$-bound **18** (C_{50} = 0.6 μM) than the consecutive G-recognizing **19** (C_{50} = 2.0 μM), while the latter **19** is more effective (C_{50} = 0.4 μM) in releasing the poly(dG)poly(dC)-bound **18** than the former **4** (C_{50} = 0.7 μM). For reference, we checked that Zn^{2+} alone (0 – 40 μM), or Zn^{2+}–cyclen (0 – 40 μM) could not displace **18** at all.

Table 10 Comparison of C_{50} (μM)[a] of **19**, actinomycin D **4** in 10 mM EPPS (pH 8.0) with I = 0.1 ($NaNO_3$) at 25 °C..

	Metal-free	Cu^{2+}-complex		
DNA	**19**	**19**	**19**	**4**
calf thymus DNA	14	1.4	1.5	1.7
poly(dG)·poly(dC)	9.0	0.4	0.5	0.7
poly(dG-dC)$_2$	16	2.0	2.8	0.6
poly(dA)·poly(dT)	29	3.3	–[b]	–[b]
poly(dA-dT)$_2$	5.5	1.9	–[b]	–[b]

[a] C_{50} values are the concentrations required for 50% decrease in the fluorescence intensity of the various DNA-bound ethidium bromide at [nucleobase in DNA] = [ethidium bromide] = 2.0 μM. The estimate errors in the C_{50} values were ±10%. [b] Not determined.

5. Interaction of Zn^{2+}–anthraquinonyl cyclen with GC boxes in SV 40 early promoter

SV40 early promoter fraction (197 bp) features T-rich sequence at "TATA box", locating at 25 – 30 bp upstream and six G-rich elements, "GC boxes", at 50 – 110 bp upstream from the transcriptional start site (Figure 17(a)). The eukaryotic RNA polymerase II machinery becomes activated for initiation of transcription after its component "TATA binding protein (TBP)" attaches to the "TATA box" and another component Sp1 protein binds to the "GC boxes".[72]

The DNase I footprinting results are obtained for the lower G and upper C strands (sense and non-sense strands for transcription, respectively, for sequence see Fig 20) in Figure 21, which showed that six GC boxes (1 – 6) of both strands were protected from DNase I hydrolysis by **19**, but the TATA box was not. Thus we were more assured of the selective recognition of GC-rich regions by **19**. Moreover, the differential DNase I cleavage plots (at [**19**] = 12.5 μM, Figure 20) indicated that the G and its C partners were not equally protected in the GC boxes: e.g., 5'-GGGCGGG-3' (in the G strand) were better protected than the pairing 5'-CCCGCCC-3' (in the C strand, see Figure 20), suggesting that in the GC pairs G is better protected probably due to the more intimate interaction of **19** with G. Zn^{2+} is essential in the interaction of **19** with the GC boxes. In the absence of Zn^{2+}, **19** (5-15 μM) did not protect these regions at all.

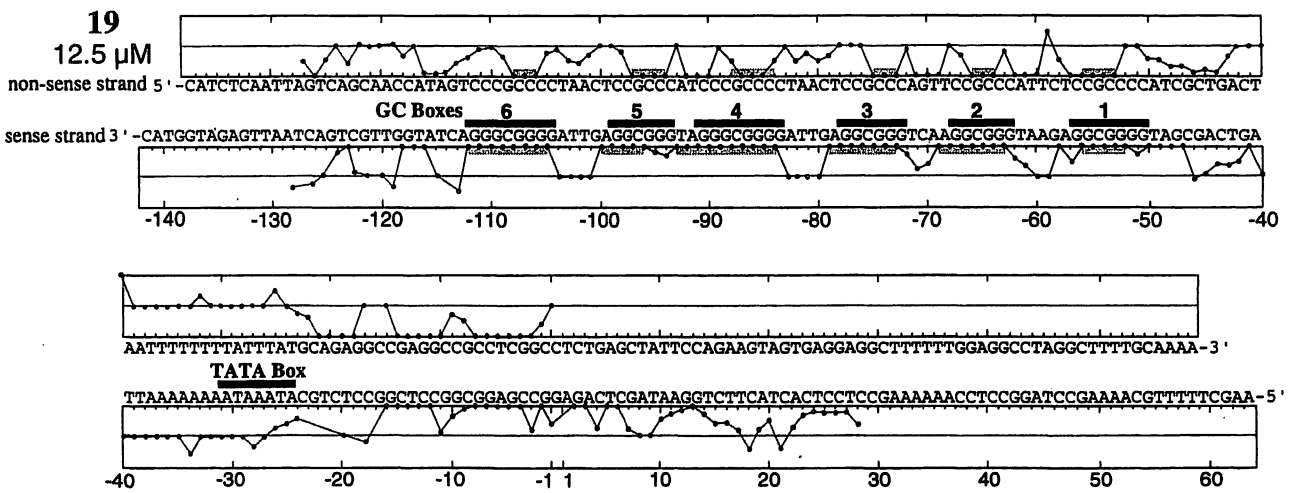

Figure 20 The sequence of the SV40 early promoter region DNA (*Bgl* II/*Hin* dIII fragment) used for the DNase I footprinting assay and differential DNase I cleavage plots in the presence of **19** (12.5 μM).

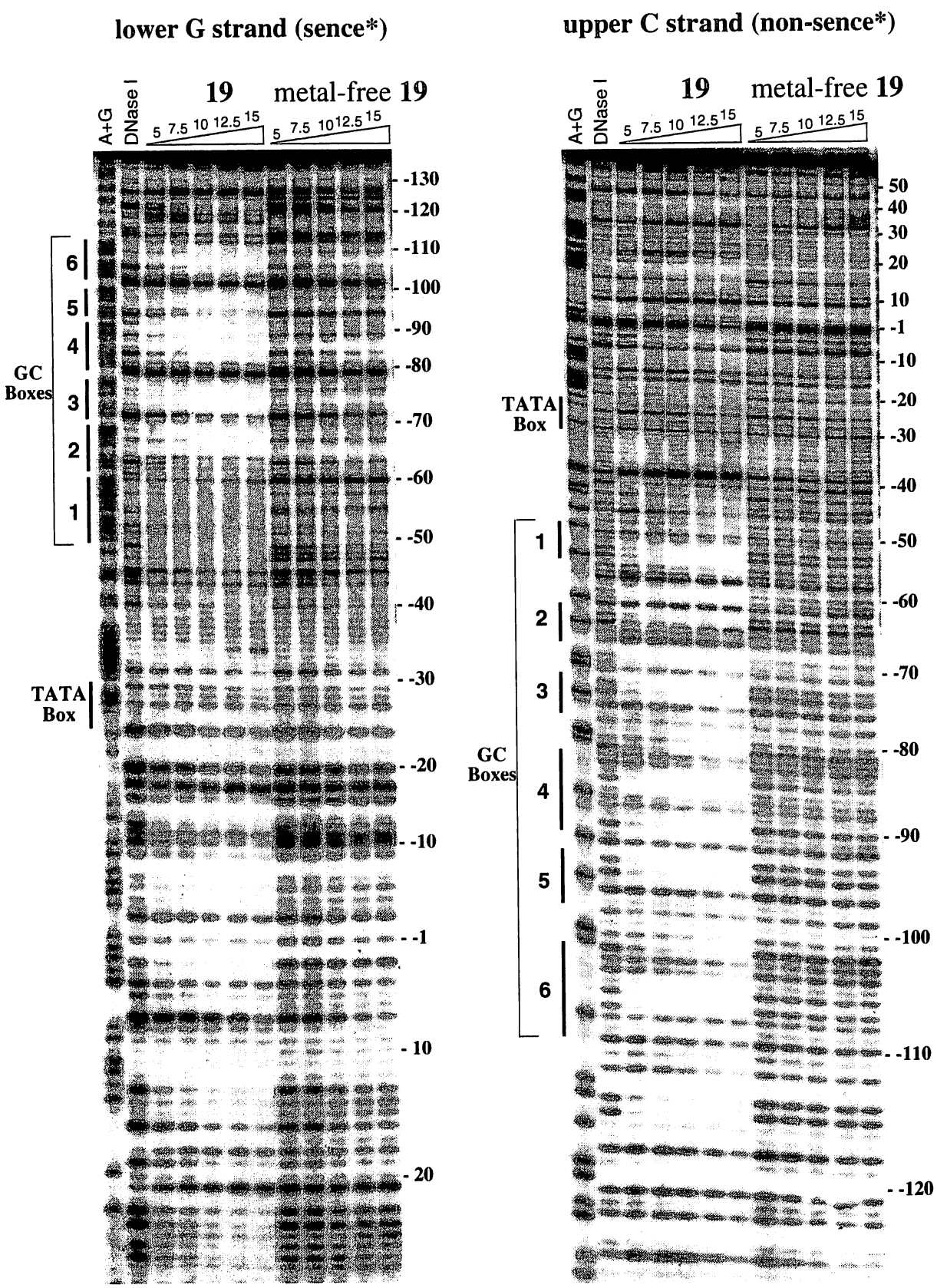

Figure 21 DNase I footprinting of SV40 early promoter region DNA in the presence of **19** and metal-free **19** (2.5, 5, 7.5, 10, 12.5, and 15 μM). The asterisk indicates which strand bears the 5'-^{32}P label (sense* = lower strand, non-sense* = upper strand shown in Figure 20). The number at the side corresponds to the distance from the transcription start site.

Inhibition of Sp1 (a GC box-specific transcriptional factor) Binding to the GC Boxes by **19**. Sp1 protein contains three contiguous repeats of a typical Cys_2His_2-type zinc finger motif, which bind to the GC boxes from the major groove (where guanine N(7) locates) of the SV 40 early promoter DNA.[72,88-91] It is thus of an extreme interest both structurally and biochemically to see how **19** that would bind to guanine N(7) competes against the Sp 1 binding to the GC boxes. Earliar, we found that human TBP was strongly inhibited from interacting with the "TATA box" in consensus DNA by the T-recognizing Zn^{2+}–cyclen complexes including **7**.

To determine the inhibitory effect of **19** on the binding of human Sp1 to GC boxes, we studied a gel mobility shift assay using a 23-bp GC box-consensus DNA fragment (for sequence, see Experimental Section). The consensus base sequence of the Sp1 binding is the 5'-(G/T)GGGCGG(G/A)(G/A)(C/T)-3' and Sp1 interacts with both strands of this DNA, but the majority of the contacts are with the G-rich strand.[90-91] Results of the gel mobility shift assay in the absence and presence of **19** and metal-free **19** are shown in Figure 22(a). With an increasing concentration (0 – 50 μM) of **19**, the density of the Sp1-bound DNA decreased. The concentration of 50% inhibition (IC_{50}) of the Sp1-DNA complex formation by **19** was estimated at 38 μM by the densitometric analysis. The metal-free **19** (0 – 50 μM) or the T-recognizing **7** and its metal-free **7** (0 – 50 μM) (Figure 22(b)) demonstrated much weaker inhibitory effect on the Sp1 binding to DNA (all $IC_{50} > 50$ μM).

To check the selective GC box specificity of **19**, we studied the inhibition of TBP binding to the 25 bp TATA box-consensus DNA by **19** and compared with the previous result for **7**. While the T-selective **7** inhibited the TBP-TATA box DNA complexation ($IC_{50} = 15$ μM), **19** showed little inhibition on the TBP binding to DNA ($IC_{50} > 50$ μM, Figure 22(c)). For comparison, actinomycin D **4** showed a more effective value ($IC_{50} = 4.6$ μM).

All these facts combined we conclude that Zn^{2+}–anthraquinonyl-cyclen **19** binds selectively to consecutive guanine bases (···GpGpGp···) in double stranded DNA, which is in contrast to the previously reported Zn^{2+}–acridinyl-cyclen **7** that selectively recognized T-rich sequence (···TpTpTp···) in DNA. Although a detailed study is needed, we tentatively propose that the G-rich sequence selectivity by **19** arose from a dominant stacking attraction between the pendant (anthraquinone) and guanine in the double helical DNA and supplementary binding between Zn^{2+}

and guanine N(7). Previously, we showed that the acridine pendant homologue **7** selectively bound to the T-rich TATA box, which was accounted for by the dominant binding of T$^-$–Zn^{2+}–cyclen and supplementary stacking between acridine and thymine (Scheme 4).

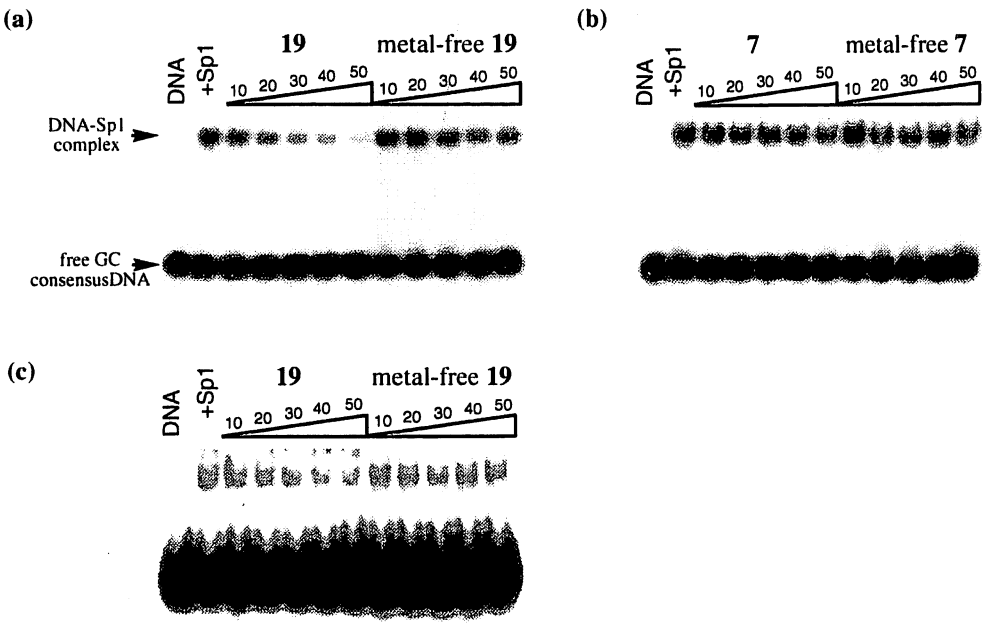

Figure 22 Gel mobility shift assay for (a) inhibition of GC box consensus DNA fragment-Sp1 complex by **19** and metal-free **19** (0 – 50 μM), (b) **7** and metal-free **7** (0 – 50 μM), and (c) inhibition of TATA box consensus DNA fragment-TBP complex by **19** and metal-free **19** (0 – 50 μM). Lane "DNA" represents DNA without Sp1 or TBP.

Scheme 4

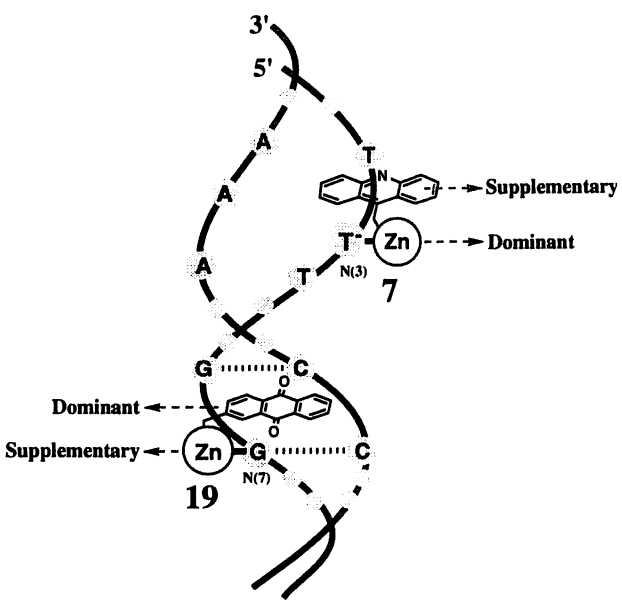

Conclusion

By the DNase I footprinting assay (Chapter I, 1-3), zinc(II)-macrocyclic tetraamine complexes appended with aromatic pendants **7**, **12**, **13**, **14**, and **15**, have been proven to selectively bind to AT-rich regions of double-stranded DNA (150 bp). The regions were almost overlapped with the sites recognized by conventional minor groove binders, distamycin A (**1**) and DAPI (**2**). The Zn^{2+}–cyclen appended with double pendants **13** and **15** showed higher affinity to the AT-rich regions than those with single pendant counterparts **12** and **13**. DNase I cleavage pattern was somewhat different for the double pendants and the single pendant systems. The Zn^{2+}–cyclen appended with single acridine-pendant **7** showed an affinity as high as **13** and **15**, and a similar DNase I cleavage pattern as **12** and **14**. Zn^{2+} is an essential metal ion for the recognition of AT-rich regions, which could not be replaced by other metal ions such as Cu^{2+} or Ni^{2+}. The vacant fifth coordination site of the Zn^{2+}–cyclen is essential, as demonstrated by the strong inhibition of the SH-containing captopril.

The footprinting by micrococcal nuclease(Chapter I, 4-5), which tends to cut pA and pT more than pC and pG and has a specific ability to nick the transiently melted DNA, revealed the fundamentally different interaction modes by the Zn^{2+}–cyclen derivatives and minor groove binders distamycin A (**1**) and DAPI (**2**). It was shown that almost all the T's in double-stranded DNA were recognized by the Zn^{2+}–cyclen derivatives, resulting in the protection of those pT bonds. On the other hand, the pairing pA's were strongly hydrolyzed. It is concluded that the Zn^{2+}–cyclen derivatives broke into the hydrogen bonds of A–T base pairs to bind to T, especially at homopolymeric AT-regions. The resulting single-stranded A region thus became exposed and came under heavy attack by the nuclease. By contrast, **1** and **2** interacted with A and T simultaneously in the same AT- regions to protect both A and T from the micrococcal nuclease hydrolysis. It was demonstrated that **1** and **12** reversibly compete for common AT-regions.

Zn^{2+}–complexes **7**, **12**, and **13** bind to double stranded calf thymus DNA and synthetic DNAs, as studied by UV and visible spectrophotometric titrations (Chapter I, 6-7). At relatively dilute concentration, the Zn^{2+}–acridinylcyclen **7** showed 31.4 and 17.2 times higher affinity for intact double-stranded homo- and hetero-AT polymers than metal-free **7**, which is to be compared with

8.8 and 4.5 times higher affinity for GC polymers. This fact suggests that the Zn^{2+}–cyclen moiety determine the preference to AT sequence over GC sequence. Stronger hypochromism and bathochromism of the absorption spectra of Zn^{2+}–cyclen complexes with DNA titration support the idea that the electrostatic interaction of the Zn^{2+}–cyclen moiety with DNA grooves bring about a closer proximity of the aromatic ring to the DNA bases. Binding of **7** to calf thymus DNA was blocked by an AT-selective, minor groove binder, distamycin (**1**), but less significantly by a major groove binder methyl green (**17**) or a intercalating agent ethidium bromide (**18**). Complex spectral changes in the titration of poly(dA)·poly(dT) by **7** at high concentration illustrates mixed equilibria including dissociation of the poly(dT) strand. From the DNA melting experiments (Chapter I, 8), it is concluded that, at lower concentration, **7** stabilized the thymine-containing DNAs predominantly by the intercalation effect of the acridine, but at higher concentration **7** destabilized the duplexes by the Zn^{2+} - (dT^-) interaction to intervene into the AT hydrogen bonds.

The DNA binding properties of the Zn^{2+}–cyclen complexes brought about inhibition of these DNA-directed transcription *in vitro* (Chapter II, 1). The Zn^{2+}–cyclen complexes, having high binding affinities to calf thymus DNA, showed the higher inhibition. Among those tested, the Zn^{2+}–bisnaphthylcyclen **15** showed the highest activity. The Zn^{2+}–acridinylcyclen **7** inhibited AT polymer-directed transcription to a greater degree than GC polymer–directed transcription, suggesting again the stronger perturbation effect on the AT duplex. The stronger uptake inhibition of ATP over UTP when the transcription was directed by the homo AT-polymer supports the stronger binding of **7** to poly(dT) strand than to poly(dA).

Among these zinc(II) complexes, **7**, **13**, and **15** effectively inhibit the DNA relaxation activity of human type II topoisomerase *in vitro* (Chapter II, 2). This result is compatible with their affinities with DNA measured by DNase I footprinting titration analysis. Moreover, in the preliminary assay, **7**, **13**, and **15** exhibited fairly strong anitimicrobial activities against gram positive bacteria (Chapter II, 3), indicating that the hydrophobic aromatic rings probably enhance the membrane permeability to effectively inhibit the bacterial growth.

By the DNase I footprinting assay, the Zn^{2+}–complexes **7**, **12**, **13**, **14**, and **15** have been proven to selectively bind to AT-rich TATA box of promoter region of SV40 early gene (Chapter II, 3). In addition, the gel mobility shift assay revealed that these zinc(II) complexes inhibit the

formation of TBP-DNA complex. Although the inhibition of TBP-DNA by these zinc(II) complexes was weaker (IC_{50} = 2.5 μM for the most effective inhibitor, **13**) than conventional minor groove binders, **1** and **2** (IC_{50} = 0.4 μM and 0.8 μM), the present findings suggest that the Zn^{2+}–cyclen derivatives might be useful as a new type of transcriptional inhibitor.

We have demonstrated that Zn^{2+}–anthraquinonylcyclen **19** binds selectively to consecutive guanine bases (···GpGpGp···) in double stranded DNA, which is in contrast to the Zn^{2+}–acridinylcyclen **7** that selectively recognized T-rich sequence (···TpTpTp···) in DNA (Chapter II, 4). On the basis of the UV spectrophotometric titirations, the Zn^{2+} complex **19** is 30 times more efficient in binding to poly(dG)poly(dC) than the metal-free **19**. In parallel, the Zn^{2+}–complex **19** drove off the poly(dG)·poly(dC)-stacked ethidium bromide (**18**) 22 times more efficiently than **7**. The consecutive G-binding property of **19** was disclosed by the K_{app} value of $1.5 \times 10^5\,M^{-1}$ for poly(dG)·poly(dC) versus $2.8 \times 10^4\,M^{-1}$ for poly(dG-dC)$_2$. This is in contrast to conventional GpC-recognizing actinomycin D (**3**), which prefers poly(dG-dC)$_2$ ($K_{app} = 1.3 \times 10^5\,M^{-1}$) over poly(dG)·poly(dC) ($K_{app} = 2.9 \times 10^4\,M^{-1}$), as measured under the same conditions. The ethidium bromide displacement study supported the efficient recognition of consecutive G by **19**.

The selective recognition of G-rich sequence, GC boxes, was shown by the DNase I footprinting of SV40 early promotor DNA (Chapter II, 5). We tentatively propose that the G-rich sequence selectivity by **19** arose from a dominant stacking attraction between the pendant (anthraquinone) and guanine in the double helical DNA and supplementary binding between Zn^{2+} and guanine N(7). In chapter I, we showed that the Zn^{2+}– acridinylcyclen **7** selectively bound to the TATA box, which was accounted for by the dominant binding of T^-–Zn^{2+}–cyclen and supplementary stacking between acridine and thymine (Scheme 4). Just as **7** inhibited interaction of a TATA binding protein with a TATA box DNA, **19** inhibited interaction of Sp1 transcriptional factor protein with GC boxes in the same DNA.

The selective and efficient T- or G- recognizing properties of the Zn^{2+}–cyclen derivatives may develop into new biochemical and medical functions at the various stages to gene expression, e.g., transcription or replication. We conclude that these Zn^{2+}–cyclen derivatives may be promising as a new type of genetic controlling factor.

Experimental Section

General Information. All reagents and solvents used were purchased at the highest commercial quality and used without purification. Aqueous solutions of 10 mM distamycin A (Sigma), 10 mM DAPI (4,6-diamidine-2-phenylindole) (Sigma), 10 mM methyl green (SIGMA), and 10 mM ethidium bromide (Merck) were prepared using deionized and distilled water and stored at –20 °C. A stock solution of 3 mM echinomycin (Sigma) and 2 mM actinomycin D (Wako) in dimethyl sulfoxide were prepared and stored at –20 °C. Concentrations of distamycin A, DAPI, methylgreen, ethidium bromide, echinomycin, and actinomycin D in aqueous solution were determined spectrophotometrically (ε_{303} = 34,000 M^{-1} cm^{-1} for distamycin A,[10] ε_{342} = 23,000 for DAPI,[14] ε_{638} = 85,300 for methyl green,[64] ε_{480} = 5,850 for ethidium bromide,[78] ε_{325} = 11,500 for echinomycin,[19] ε_{440} = 24,450 for actinomycin D[22]).

All the cyclen derivatives except for **15** and its metal-free ligand were dissolved in 10 mM EPPS (pH 8.0). **15** and its metal-free ligand were dissolved in 10 mM EPPS (pH 8.0) containing 50 % dimethylsulfoxide. Concentrations of cyclen complexes were determined spectrophotometrically; ε_{361} = 10,030 for **7**, ε_{361} = 9,980 for metal-free **7**, ε_{334} = 9,980 for Cu^{2+}–complex **7**, ε_{317} = 3,900 for **12**, ε_{316} = 3,100 for metal-free **12**, ε_{317} = 7,400 for **13**, ε_{316} = 6,200 for metal-free **13**, ε_{283} = 7,000 for **14**, ε_{283} = 6,800 for metal-free **14**, ε_{283} = 15,300 for **15**, ε_{283} = 12,300 for metal-free **15**, ε_{334} = 6,640 for **19**, ε_{334} = 5,420 for metal-free **19**, and ε_{334} = 6,330 for Cu^{2+}–complex **19**.

Calf thymus DNA (SIGMA) was dissolved in water, sonicated, and filtered. Poly(dA)·poly(dT), poly(dA-dT)$_2$, poly(dC)·poly(dG), poly(dC-dG)$_2$, poly(dI)·poly(dC), poly(dI-dC)$_2$, poly(dA), and poly(dT) (all Amersham Pharmacia) were dissolved in water. Their concentrations per phosphates were determined spectrophotometrically; ε_{253} = 6,600 for calf thymus DNA,[92] ε_{260} = 6,000 for poly(dA)·poly(dT),[92] ε_{262} = 6,600 for poly(dA-dT)$_2$,[93] ε_{253} = 7,400 for poly(dG)·poly(dC),[92] ε_{254} = 8,400 for poly(dG-dC)$_2$,[92] ε_{254} = 5,300 for poly(dI)·poly(dC),[94] and ε_{251} = 6,900 for poly(dI-dC)$_2$,[95] ε_{257} = 8,600 for poly(dA),[96] and ε_{264} = 8,520 for poly(dT).[97] They were stored at -20°C in a final concentration of 1mM per phosphates in 10 mM EPPS (pH 8.0) containing 0.1M $NaNO_3$.

DNase I (Takara Shuzo) and micrococcal nuclease (Worthington Biochemical Corporation) were diluted to 0.03 unit/μL in aqueous solution containing 2.5 mM $CaCl_2$ and 5 mM $MgCl_2$, and stocked at –20 °C.

The synthesis of an acridinyl-cyclen hydrochloric acid salt, **7**·4HCl· $4H_2O$ and its zinc(II) complex **7**·4HCl·$4H_2O$ is reported in ref. 39, and an anthraquinonyl-cyclen trihydrochloric acid salt, metal-free **19**·3HCl and its zinc(II) complex **19**·$(NO_3)_2$ is reported in ref. 47. The copper(II) complex **7** and **19** were prepared by mixing the calculated amount of 5 mM $CuSO_4 \cdot 5H_2O$ (99.99% purity) with equimolar metal-free ligand **7** and **19** in a buffer solution (pH > 7).

UV spectra were recorded on a Hitachi U–3500 spectrophotometer at 25 °C. IR spectra were recorded on a Shimadzu FTIR–4200 spectrophotometer at room temperature. ^{1}H(500 MHz) and ^{13}C(125 MHz) NMR spectra at 35°C were recorded on a JOEL LA500 spectrometer. 3-(Trimethylsilyl)propionic-2,2,3,3-d_4 acid sodium salt in D_2O and tetramethylsilane in DMSO-d_6 were used as internal references for NMR measurements. Elemental analysis was performed on a Perkin Elmer CHN Analyzer 2400. Silica gel column chromatography was performed using Fuji Silysia Chemical FL–100D.

Synthesis of Zn^{2+}–(4-Quinolyl)methyl-cyclen, 12·$(NO_3)_2$. An acetonitrile solution (120 mL) of 4-(chloromethyl)-quinoline (774 mg, 4.36 mmol) and 1,4,7,10-tetraazacyclododecane (1.50 g, 8.71 mmol) was stirred for 12 h at 70 °C. After evaporation of the solvent, the residue was purified by silica gel column chromatography (CH_2Cl_2/MeOH/28% aqueous NH_3 = 10:1:0.1) followed by crystallization from aqueous 48% HBr/MeOH to obtain colorless needles of (4-quinolyl)methyl-cyclen·4HBr·$2H_2O$ (1.11 g, 45% yield). IR (KBr pellet): 3425, 3005, 2722, 1599, 1441, 1415, 1291, 1221, 1074, 831, 527 cm^{-1}. ^{1}H NMR (D_2O, 55 °C): δ 3.04 (4H, t, J = 5.1 Hz, NCH_2), 3.08 (4H, t, J = 5.1 Hz, NCH_2), 3.22 (4H, t, J = 4.9 Hz, NCH_2), 3.31 (4H, t, J = 4.9 Hz, NCH_2), 4.63 (2H, s, $ArCH_2$), 8.03 (1H, m, ArH), 8.10 (1H, d, J = 5.5 Hz, ArH), 8.19 (1H, m, ArH), 8.28 (1H, d, J = 8.5 Hz, ArH), 8.44 (1H, d, J = 9.5 Hz, ArH) , 9.10 (1H, d, J = 5.5 Hz, ArH). ^{13}C NMR (D_2O): δ 44.5, 45.3, 47.5, 51.6, 56.4, 124.2, 124.4, 127.4, 130.9, 133.5, 138.1, 140.2, 146.3, 159.0. Anal. Calcd for $C_{18}H_{35}N_5O_2Br_4$: C, 32.1; H, 5.2; N, 10.4. Found: C, 32.2; H, 5.3; N, 10.3.

The solution pH of (4-quinolyl)methyl-cyclen·4HBr·$2H_2O$ (600 mg, 0.891 mmol) in 10 mL

H_2O was adjusted to 12 with 5 M NaOH. The alkaline solution was extracted with CH_2Cl_2 (50 mL × 8) and then the organic solvent was evaporated. An EtOH solution (10 mL) of the obtained acid-free ligand and $Zn(NO_3)_2 \cdot 6H_2O$ (280 mg, 0.941 mmol) was stirred at room temperature for 1 h. After evaporation of the solvent, the residue was crystallized from H_2O/EtOH to obtain colorless needles of **12**·$(NO_3)_2$ (357 mg, 80 % yield). IR (KBr pellet): 3206, 1468, 1385 (NO_3^-), 1302, 1086, 978, 775 cm^{-1}. ^1H NMR (D_2O): δ 2.80–2.92 (8H, m, NCH_2), 2.95–3.10 (6H, m, NCH_2), 3.20–3.35 (2H, m, NCH_2), 4.57 (2H, s, $ArCH_2$), 7.63 (1H, d, J = 4.5 Hz, ArH), 7.80 (1H, dd, J = 6.5 and 8.5 Hz, ArH), 7.93 (1H, dd, J = 6.5 and 8.5 Hz, ArH), 8.17 (1H, d, J = 8.5 Hz, ArH), 8.28 (1H, d, J = 8.5 Hz, ArH) , 8.90 (1H, d, J = 4.5 Hz, ArH). ^{13}C NMR (D_2O): δ 45.3, 46.5, 47.6, 52.8, 53.6, 126.5, 127.1, 130.68, 130.73, 131.4, 133.3, 142.4, 149.9, 152.2. Anal. Calcd for $C_{18}H_{27}N_7O_6Zn$: C, 43.0; H, 5.4; N, 19.5. Found: C, 43.1; H, 5.5; N, 19.6.

Synthesis of Zn^{2+}–1,7-Bis((4-quinolyl)methyl)-cyclen, 13·$(NO_3)_2 \cdot H_2O$. An acetonitrile solution (120 mL) of 4-(chloromethyl)-quinoline (2.40 g, 13.5 mmol), K_2CO_3 (1.90 g, 13.7 mmol), and 1,7-bis(diethoxyphosphoryl)-1,4,7,10-tetraazacyclododecane (2.00 g, 4.5 mmol)[98] was refluxed for 1 day. After removal of inorganic salts, the solvent was evaporated. The residue was purified by silica gel column chromatography (eluent: CH_2Cl_2/MeOH = 25:1). After evaporation of the solvent, MeOH (15 mL) and 36% aqueous HCl (5 mL) were added. The reaction mixture was stirred at 60 °C for 12 h. After evaporation of the solvent, the residue was dissolved in H_2O (20 mL) and the solution pH was adjusted to 12 with 5 M NaOH. The alkaline solution was extracted with CH_2CH_2 (100 mL × 5) and the solvent was evaporated. The residue was crystallized from 48% aqueous HBr/MeOH to obtain 1,7-bis((4-quinolyl)methyl)-cyclen·4HBr·$2H_2O$ as colorless prisms (1.33 g, 36% yield). IR (KBr pellet): 3351, 2635, 1599, 1389, 1343, 1051, 822, 612 cm^{-1}. ^1H NMR (D_2O): δ 3.25 (8H, t, J = 5.0 Hz, NCH_2), 3.44 (8H, t, J = 5.0 Hz, NCH_2), 4.84 (4H, s, $ArCH_2$), 8.07 (2H, dd, J = 6.5 and 8.5 Hz, ArH), 8.15 (2H, d, J = 5.5 Hz, ArH) 8.22 (2H, dd, J = 6.5 and 8.5 Hz, ArH), 8.31 (2H, d, J = 8.5 Hz, ArH), 8.52 (2H, d, J = 8.5 Hz, ArH), 9.15 (2H, d, J = 5.5 Hz, ArH). ^{13}C NMR (D_2O): δ 46.1, 50.7, 55.6, 124.52, 124.54, 127.5, 131.1, 133.4, 137.9, 140.7, 146.4, 157.6. Anal. Calcd for $C_{28}H_{42}N_6O_2Br_4$: C, 41.3; H, 5.2; N, 10.3. Found: C, 41.3; H, 5.3; N, 10.2.

Zinc(II) complex **13**·$(NO_3)_2$·H_2O as colorless prisms was obtained in 70 % yield by almost the same method as used for **12** except using the H_2O/MeOH for its crystallization. IR (KBr pellet): 3223, 1491, 1385 (NO_3^-), 1287, 1092, 772 cm^{-1}. ^1H NMR (D_2O): δ 2.86–2.91 (4H, m, NCH_2), 2.97–3.05 (4H, m, NCH_2), 3.00–3.15 (4H, m, NCH_2), 3.35–3.41 (4H, m, NCH_2), 4.60 (4H, s, $ArCH_2$), 7.82 (2H,d, J = 4.5 Hz, ArH), 7.84 (2H, dd, J = 6.5 and 8.5 Hz, ArH), 7.96 (2H, dd, J = 6.5 and 8.5 Hz, ArH), 8.19 (2H, d, J = 8.5 Hz, ArH), 8.29 (2H, d, J = 8.5 Hz, ArH), 8.94 (2H, d, J = 4.5 Hz, ArH). ^{13}C NMR (DMSO-d_6): δ 43.0, 49.3, 50.6, 123.75, 123.84, 127.0, 127.6, 129.3, 129.9, 138.3, 148.1, 149.8. Anal. Calcd for $C_{28}H_{36}N_8O_7Zn$: C, 50.8; H, 5.5; N, 16.9. Found: C, 51.2; H, 5.6; N, 16.9.

Synthesis of Zn^{2+}–(1-Naphthyl)methyl-cyclen, 14·$(NO_3)_2$. An acetonitrile solution (60 mL) of 1-(chloromethyl)-naphthalene (934 mg, 5.29 mmol) and 1,4,7-tris(*tert*-butyloxycarbonyl)-1,4,7,10-tetraazacyclododecane[99] (1.00 g, 2.12 mmol) was refluxed in the presence of K_2CO_3 (730 mg, 5.29 mmol) for 1 day. After removal of inorganic salts, the solvent was evaporated. The residue was purified by silica gel column chromatography (eluent; CH_2Cl_2/MeOH = 50:1). After evaporation of the solvent, the residue was dissolved in EtOH (10 mL) and then 48% aqueous HBr (2 mL) was added. The reaction mixture was stirred for 12 h at room temperature. After evaporation of the solvent, the residue was crystallized from 48% aqueous HBr/MeOH to obtain colorless needles of (1-naphthyl)methyl-cyclen·3HBr·H_2O (0.742 mg, 61% yield). IR (KBr pellet): 2953, 2705, 1597, 1443, 1069, 781 cm^{-1}. ^1H NMR (D_2O): δ 2.92 (4H, br, NCH_2), 3.02–3.04 (8H, m, NCH_2), 3.12 (4H, br, NCH_2), 4.35 (2H, s, $ArCH_2$), 7.58–7.67 (3H, m, ArH), 7.71 (1H, t, J = 7.5 Hz, ArH), 8.02 (1H, d, J = 8.0 Hz, ArH) 8.07–8.09 (2H, m, ArH). ^{13}C NMR (D_2O): δ 44.8, 45.2, 47.0, 52.5, 58.9, 125.5, 128.9, 129.5, 130.2, 132.4, 132.5, 132.6, 134.1, 134.4, 136.8. Anal. Calcd for $C_{19}H_{33}N_4OBr_3$: C, 39.8; H, 5.8; N, 9.8. Found: C, 40.0; H, 5.9; N, 9.8.

Zinc(II) complex **14**·$(NO_3)_2$ as colorless prisms was obtained in 53 % yield by almost the same method as used for **12**. IR (KBr pellet): 3204, 1495, 1385 (NO_3^-), 1092, 980, 791 cm^{-1}. ^1H NMR (D_2O): δ 2.59–2.64 (2H, m, NCH_2), 2.76–2.88 (6H, m, NCH_2), 2.93–3.04 (6H, m, NCH_2), 3.20–3.26 (2H, m, NCH_2), 4.48 (2H, s, $ArCH_2$), 7.58–7.71 (4H, m, ArH), 8.02–8.05 (2H, m, ArH), 8.21 (1H, d, J = 8.5 Hz, ArH). ^{13}C NMR (D_2O): δ 45.3, 46.5, 47.5, 52.7, 54.5, 126.2, 128.2, 129.1,

129.9, 131.2, 132.0, 132.4, 133.5, 135.5, 136.6. Anal. Calcd for $C_{19}H_{28}N_6O_6Zn$: C, 45.5; H, 5.6; N, 16.8. Found: C, 45.8; H, 5.6; N, 16.5.

Synthesis of Zn^{2+}–1,7-Bis((1-naphthyl)methyl)-cyclen, 15·$(NO_3)_2$. 1,7-Bis((1-naphthyl)methyl)-cyclen·2HBr·H_2O as colorless prisms was obtained in 40.0% yield by almost the same method as used for **13**. IR (KBr pellet): 3436, 2953, 2768, 1466, 1395, 783 cm^{-1}. ^1H NMR (DMSO-d_6): δ 2.92 (8H, br, NCH_2), 3.21 (8H, br, NCH_2), 4.32 (4H, s, $ArCH_2$), 7.56–7.67 (8H, m, ArH), 7.95 (2H, d, J = 7.9 Hz, ArH), 8.01 (2H, d, J = 7.6 Hz, ArH), 8.26 (2H, d, J = 8.6 Hz, ArH). ^{13}C NMR (DMSO-d_6): δ 42.5, 47.8, 52.8, 123.4, 125.4, 125.7, 126.5, 127.98, 128.05, 128.8, 132.0, 132.1, 133.5. Anal. Calcd for $C_{30}H_{40}N_4OBr_2$: C, 57.0; H, 6.4; N, 8.9. Found: C, 57.1; H, 6.3; N, 8.9.

Zinc(II) complex **15**·$(NO_3)_2$ was obtained as colorless prisms in 68.0 % yield by almost the same method as used for **12** except using the H_2O/CH_3CN for its crystallization. IR (KBr pellet): 3189, 1945, 1385 (NO_3^-), 1096, 1013, 785 cm^{-1}. ^1H NMR (DMSO-d_6): δ 2.50–2.57 (4H, m, NCH_2), 2.74–2.87 (4H, m, NCH_2), 2.91–3.01 (4H, m, NCH_2), 3.05–3.20 (4H, m, NCH_2), 4.48 (4H, s, $ArCH_2$), 7.58–7.70 (8H, m, ArH), 8.00–8.03 (4H, m, ArH), 8.28 (2H, d, J = 8.3 Hz, ArH). ^{13}C NMR (DMSO-d_6): δ 43.0, 49.0, 51.1, 123.6, 125.1, 125.8, 126.6, 128.7, 128.9, 129.0, 130.4, 132.6, 133.6. Anal. Calcd for $C_{30}H_{36}N_6O_6Zn$: C, 56.1; H, 5.7; N, 13.1. Found: C, 56.4; H, 5.8; N12.7.

DNase I and Micrococcal Nuclease Footprintings for 150 bp DNA fragment. The 150 bp DNA fragments (pUC19 sequence from 1881 to 2030 (AT-rich region) was arbitrarily selected) was amplified by PCR using pUC19 as a template and two 20 mer primers (5'GCGTCAGACCCCGTAGAAAA3' and 5'AGTTACCTTCGGAAAAAGAG3') obtained from Amersham Pharmacia Biotech. The 5'-end of either primer (Watson or Crick strand) was 5'-^{32}P labeled with T4 polynucleotide kinase and [γ-^{32}P] ATP. The amplified DNA fragments were purified by non-denatured polyacrylamide gel electrophoresis.

The 5'-^{32}P labeled 150 bp DNA fragment (10,000 cpm) and sonicated calf thymus DNA (100 μM base) were incubated with a testing compounds in 50 μL of 10 mM EPPS (pH 8.0) at 25 °C for an hour. Then 0.09 unit of DNase I or micrococcal nuclease was added and incubated for 3 min

at room temperature. Digestion was quenched by addition of 10 μL solution containing 50 mM EDTA, 0.5%(w/v) sodium dodecyl sulfate (SDS), 1.8 M sodium acetate, and 10 μg yeast tRNA. The cleaved DNA was ethanol precipitated, dried and dissolved in 3 μL of 95%(v/v) formamide/H_2O containing 0.05%(w/v) bromophenol blue, 0.05%(w/v) xylene cyanol, and 20 mM EDTA. They were heated at 95 °C for 10 min and loaded onto denatured 8%(w/v) polyacrylamide gel. After drying the gel, autoradiography was carried out at –80°C without using intensifying screen. Bands in the digests were assigned by comparison with Maxam-Gilbert markers specific for adenine and guanine.[100] The densitometric analysis was carried out using BIO-1D software from M&S Instruments Trading Inc. The footprintings were performed at least three times.

UV and Visible Absorption Studies Spectrophotometric titration experiments were performed with a HITACHI U-3500 spectrophotometer at 25°C. Quartz cuvett (1 cm) was used, with continuous stirring throughout the course of the titration. A stock solution of DNAs (1.0 mM per phosphates in 10 mM EPPS (pH 8.0) containing 0.1 M $NaNO_3$) was added in increasing amounts to a 2 ml solution of the tested compounds in the same buffer. The decreases in the absorption of the compounds at their absorption maxima were measured. The apparent binding constants K_{app} were determined from the plots of $D / \Delta\varepsilon_{app}$ versus D, where D is the concentration of DNA in phosphates, $\Delta\varepsilon_{app} = \varepsilon_f - \varepsilon_{app}$, and $\Delta\varepsilon = \varepsilon_f - \varepsilon_b$,[61] where ε_b and ε_f correspond to the extinction coefficient of the DNA-bound compounds and the extinction coefficient of the DNA-unbound compounds, respectively. The apparent extinction coefficient, ε_{app}, was obtained by calculating A_{obsd} / [compounds], where A_{obsd} corresponds to the observed absorbance at absorption maxima. The data were fitted to eq.1, wherein a slope equal to $1 / \Delta\varepsilon$ and a y-intercept equal to $K_{app} / \Delta\varepsilon$ were obtained. ε_b was determined from $\Delta\varepsilon$, and K_{app} from the ratio of the slope to the y-intercept.

$$D / \Delta\varepsilon_{app} = D / \Delta\varepsilon + K_{app} / \Delta\varepsilon \quad (1)$$

The concentration of the DNA-bound compounds (C_b) was determined as follow.[101]

$$C_b = (\varepsilon_f \cdot C_{total} - A_{obs}) / (\varepsilon_f - \varepsilon_b) \quad (2)$$

The concentration of the DNA-unbound compounds (C_f) was determined by

$$C_f = C_{total} - C_b \quad (3)$$

DNA Melting Studies Thermal melting curves of native and synthetic DNAs (50 μM in 10 mM EPPS buffer (pH 8.0 at 25 °C) containing 15 mM $NaNO_3$) were followed on a HITACHI U-3500 spectrophotometer equipped with a thermoelectric cell temperature controller (± 0.5°C) and a stirrer unit. A 1cm quartz cuvett was used. The temperature was raised at the rate of 0.5°C / min. T_m values were determined by differentiation of the melting curves. The ΔT_m value for each compound was calculated as the temperature difference between the compound's T_m and the DNA's T_m.

DNA Transcription Inhibition Assay The inhbitory activities of Zn^{2+}–cyclen complexes in transcription of DNA *in vitro* were examined using calf thyums DNA or synthetic DNA polymers as a template and *E.coli* RNA polymerase (from SIGMA).[23] Reaction mixtures (total volume 50 μl) contained each 200 μM of GTP, CTP, ATP, and UTP except where [^{3}H] UTP (50 mCi / mmol, 200 μM), [^{3}H] ATP (50 mCi / mmol, 200 μM), or [α-^{32}P] CTP (6 Ci / nmol, 200 μM) were substituted for non radio-active substrate, 10 mM $MgCl_2$, and 0.2 mM dithiothreitol, template DNAs, and cyclen derivatives in 50 mM Tris HCl (pH 8.0). The phosphate concentration of the template DNAs were as follows: calf thymus DNA, 250 μM; poly(dA)·poly(dT), 20 μM; poly(dA-dT)$_2$, 20 μM; poly(dG-dC)$_2$, 20 μM. The reactions were started by adding 5 μl of RNA polymerase (0.22 μg protein / μl). All the reactions were terminated after 60 minutes at 37°C by pouring the 50 μl of the reaction solution on a DE81 filter (DEAE cellulose ion exchanger from Whatman). Filters were dried for 10 min and washed four times for 10 min with 5% Na_2HPO_4 solution. The incorporation of the labeled substrates into the synthesized RNA was counted with a liquid scintillation counter.

Antimicrobial Test. Antimicrobial activities against a gram positive bacteria (*Staphylococcus aureus* FDA 209P) and a gram negative bacteria (*Escherichia coli* NIHJ) were determined by a microtiter plate method: 0.2 ml of Müeller-Hinton broth (Oxoid) per well, an inoculum density of 1×10^5 to 5×10^5 bacteria per mL, and a range of tested compounds concentrations (0 – 50 μM) were used. After the test solutions were incubated for 12 h at 37°C, the minimum inhibitory concentrations (MICs) were determined. The MIC (μM) is defined as

the lowest concentration that inhibited growth of the bacteria.

Topoisomerase Assay. Type I topoisomerase reactions were conducted in 10 mM Tris buffer (pH 7.9, 20 μL) containing 0.25 μg of pBR 322 plasmid, 150 mM NaCl, 1 mM spermidine, 0.5 mM dithiothreitol, 100 μg/mL bovine serum albumin, and a Zn^{2+}–cyclen derivative. After addition of 0.5 unit of human type I topoisomerase (Topo GEN), the mixture was incubated for 10 min at 37 °C. Type II topoisomerase reactions were conducted in 50 mM Tris buffer (pH 8.0, 10 μL) containing 0.25 μg of pBR 322 plasmid, 120 mM KCl, 10 mM $MgCl_2$, 0.5 mM ATP, 0.5 mM dithiothreitol, 30 μg/mL bovine serum albumin, and a Zn^{2+}–cyclen derivative. After addition of 0.2 unit of human type II topoisomerase (Topo GEN), the mixture was incubated for 2 h at 37°C. Both enzyme reactions were stopped by adding phenol/chlololform (= 3:1) solution. The reacted plasmid DNA in the aqueous phase was separated from the organic phase. The composition of DNA was analyzed by electrophoresis on 1 % agarose gel containing 40 mM Tris (pH 8.0), 40 mM acetate, 1 mM EDTA, and 2 μg/mL chloloquine.

DNase I Footprinting for SV40 early gene promoter DNA fragment. A 197-bp DNA fragment form the promoter region of SV 40 was prepared by digestion of plasmid pGL control vector (Promega) by *Bgl* II (or *Hin* dIII), dephosphrylated with calf intestinal alkaline phosphatase, and 5'-^{32}P labeled with T4 polynucleotide kinase and [γ-^{32}P] ATP. Then the labeled fragment was digested with *Hin* dIII (or *Bgl* II) to generate the unique end-labeled fragment, and the desired fragment was purified by 10 % non-denatured polyacrylamide gel electrophoresis.

The 5'-^{32}P labeled SV40 early promoter DNA fragment (10,000 cpm) and a tested cycken complexes (or a recombinant human TATA box binding protein (Santa Crutz Biotechnology)) were dissolved in 25 mM Tris buffer (50 μL, pH 8.0) containing 6.25 mM $MgCl_2$, 50 mM KCl, 10 %(w/v) glycerol, 0.01 %(w/v) Nonidet P-40, 10 μM EDTA, and 20 μM dithiothreitol. After incubation for 1 h at 25 °C, 0.09 unit of DNase I was added. The mixture was incubated for 3 min at room temperature and then an aqueous solution (10 μL) containing 50 mM EDTA, 0.5 %(w/v) sodium dodecyl sulfate (SDS), 1.8 M sodium acetate, and 10 μg yeast tRNA was added. The cleaved DNA was treated with phenol/chloroform (= 3:1), precipitated with ethanol,

dried and dissolved in 3 μL of 95 %(v/v) formamide/H_2O containing 0.05 %(w/v) bromophenol blue, 0.05 %(w/v) xylene cyanol, and 20 mM EDTA. Electrophoesis of DNAs was carried out in the same method of footprinting analysis for 150 bp DNA fragment.

Gel Mobility Shift Assay for Complexation of TBP with TATA Box DNA. The 25-bp DNA (10,000 cpm, 5'-^{32}P labeled 5'-GCAGAGCATATAAAAATGAGGTAGG-3' (Santa Crutz Biotechnology)) was incubated with a Zn^{2+}–cyclen derivative for 30 min at 30 °C in 20 mM HEPES-KOH buffer (pH 7.9, 8.4 μL) containing 25 mM KCl, 2 mM spermidine, 0.025 %(w/v) nonidet P-40, 10 %(w/v) glycerol, and 100 μg/mL BSA. To the solution was added the same buffer solution (1.6 μL) containing 40 ng of a humam TATA box binding protein (Santa Crutz Biotechnology), 2.5 mM EDTA, and 0.5 mM dithiothreitol. After 30-min incubation, the mixture (10 μL) were applied onto a 6 %(w/v) native polyacrylamide gel (acrylamide/bis-acrylamide = 40/1) and run in the buffer (22.3 mM Tris, 22.3 mM boric acid, 0.5 mM EDTA, 2.5 mM $MgCl_2$, and 0.05 %(w/v) nonidet P-40) at 25°C, and analyzed by autoradiography. The densitometric analysis was carried out using BIO-1D software from M&S Instruments Trading Inc.

Ethidium Bromide Displacement Assay. Ethidium bromide **18** and DNA (both 2 μM) in 2.5 mL of buffer solution (10 mM EPPS, pH 8.0) was titrated with 1 μL aliquots of 1 mM cyclen complexes in the same buffer. The decrease in the fluorescence intensity (excitation at 520 nm and emission at 600 nm) was monitored by Hitachi U-4500 florescence spectrophotometer with I = 0.1 ($NaNO_3$) at 25°C. The measured fluorescence intensity was corrected by subtracting the intensity of the ethidium bromide (2 μM) in the absence of DNA. The C_{50} value was determined as the cyclen complex concentration required to reduce the fluorescence intensity to 50%.

Gel Mobility Shift Assay for Complexation of Sp1 with GC Box DNA. The 23-bp Sp1 consensus DNA (5'ATTACGATCGGGGCGGGGCGAGC3') (Promega) was 5'-^{32}P labeled with T4 polynucleotide kinase and [γ-^{32}P] ATP. The labeled DNA (5 nM) was incubated with a testing cyclen complex or a drug for 30 min at 25 °C in 50 mM Tris-HCl buffer (pH 7.5, 9 μL) containing 50 mM NaCl, 4 %(w/v) glycerol, and 1 mM $MgCl_2$. To the solution was added 1 μL

(86.3 ng) of humam Sp 1 (Promega, stocked in 12 mM HEPES-KOH (pH 7.5), 50% glycerol, 50 mM KCl, 6 mM $MgCl_2$, 0.1 %(w/v) Nonidet P-40, 5 μM $ZnSO_4$, and 2 mM dithiothreitol). After 30-min incubation, the mixture (10 μL) were applied onto a 4%(w/v) native polyacrylamide gel (acrylamide/bis-acrylamide = 80/1) and run in the 0.5 × TBE buffer (22.3 mM Tris, 22.3 mM boric acid, 0.5 mM EDTA) at 25°C, and analyzed by autoradiography. The densitometric analysis was carried out using BIO-1D software from M&S Instruments Trading Inc.

Appendix: Equibrium for complexation of Zn^{2+}–cyclen complex with nucleotide, and calculation of conditional binding constant (K_{app}) at various pH.

(1) Equibrium for complexation of Zn^{2+}–cyclen with dT(U).

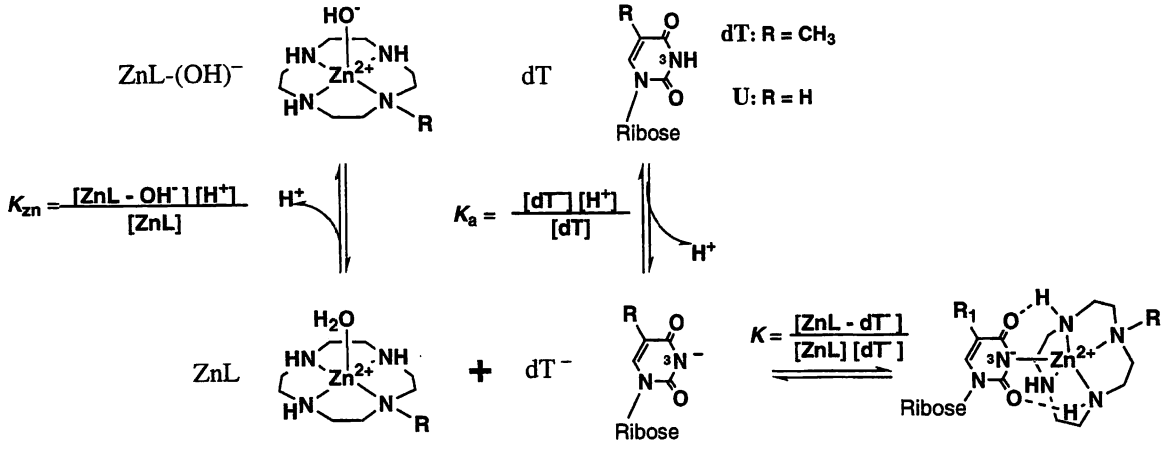

$$K_{app} = \frac{[ZnL - dT^-]}{[ZnL + ZnL(OH^-)][dT^- + dT]}$$

$$= K \times \frac{1}{(1 + \frac{K_{zn}}{[H^+]})(1 + \frac{[H^+]}{K_a})}$$

(2) Equibrium for complexation of Zn^{2+}–cyclen with dG.

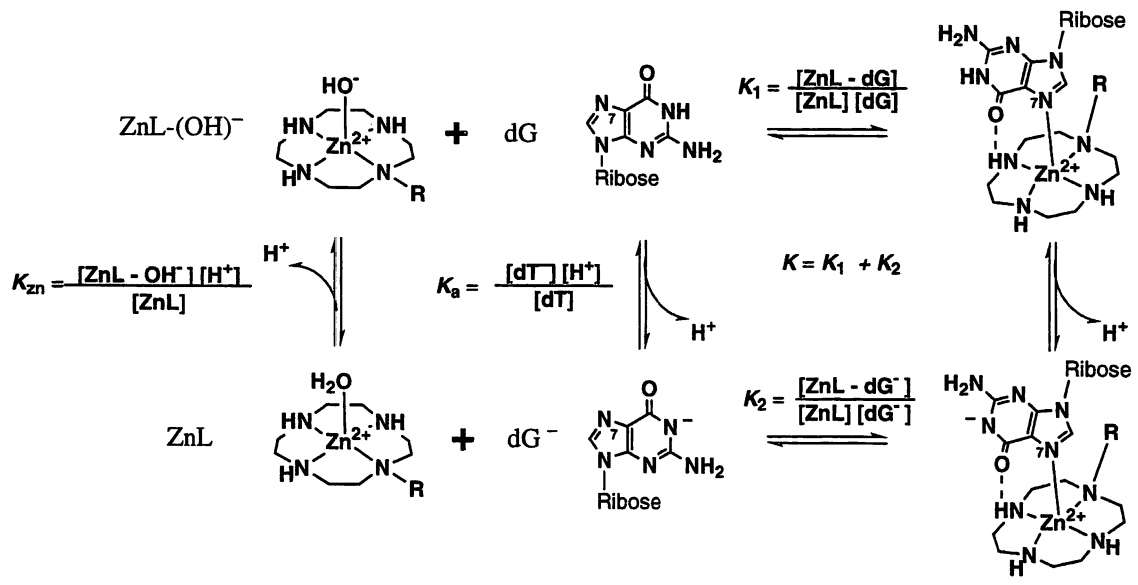

$$K_{app} = \frac{[ZnL - dG] + [ZnL - dG^-]}{[ZnL + ZnL(OH^-)][dG^- + dG]}$$

$$= K \times \left(\frac{1}{(1 + \frac{K_a}{[H^+]})(1 + \frac{K_{zn}}{[H^+]})} + \frac{1}{(1 + \frac{K_{zn}}{[H^+]})(1 + \frac{[H^+]}{K_a})} \right)$$

References and Notes

(1) Zimmer, C. and Wähnert, U. Nonintercalating DNA-binding ligands: specificity of the intercalation and their use as tools in biophysical, biochemical and biological investigations of the genetic material. *Prog. Biophys. Mol. Biol.* **1986**, *47*, 31–112.

(2) Denison, C. and Kodadek, T., Small-molecule-based strategies for controlling gene expression. *Chemistry & Biology,* **1998**, *5*, R129–R145.

(3) Coll, M.; Frederick, C. A.; Wang, A. H. J.; Rich, A., A bifurcated hydrogen-bonded conformation in the d(A-T) base pairs of the DNA dodecamer d(CGCAAATTTGCG) and its complex with distamycin. *Proc. Natl. Acad. Sci. USA* **1987**, *84*, 8385–8389.

(4) van Dyke, M. W.; Hertzberg, R. P.; Dervan, P. B., Map of distamycin, netropsin, and actinomycin binding sites on heterogeneous DNA: DNA cleavage-inhibition patterns with methidiumpropyl-EDTA·Fe(II). *Proc. Natl. Acad. Sci. USA* **1982**, *79*, 5470–5474.

(5) Fox, K. R. and Waring, M. J., DNA structural variations by actinomycin and distamycin as revealed by DNase I footprinting. *Nucleic Acid Res.* **1984**, *12*, 9271–9285.

(6) van Dyke, M. W. and Dervan, P. B., Methydiumpropyl-EDTA·Fe(II) and DNase I footprinting report different small molecule binding site size on DNA. *Nucleic Acid Res.* **1983**, *11*, 5555–5567.

(7) Griffin, J. H. and Dervan, P.B., Metalloregulation in the sequence specific binding of synthetic molecules to DNA. *J. Am. Chem. Soc.* **1987**, *109*, 6840–6842.

(8) Woynarowski, J. M.; Sigmund, R. D.; Beerman, T. A., DNA mnor groove binding agents interfere with topoisomerase II mediated lesions induced by epipodophyllotoxin derivertive VM-26 and avridine derivatives m-AMSA in nuclei from L1210 cells. *Biochemistry* **1989**, 28, 3850–3855.

(9) Wilson, W. D.; Ratmeyer, L.; Zhao, M.; Strekowski, L.; Boykin, D. The search for structure-specific nucleic acid-interactive drugs: effects of compound structure on RNA versus DNA interaction strength. *Biochemistry* **1993**, *32*, 4098–4104.

(10) Breslauer, K. J.; Remeta, D. P.; Chou, W-Y.; Ferrante, R.; Curry, J.; Zaunczkowski, D.; Synder, J. G.; Marky, L. A., Enthalpy-entropy compensations in drug-DNA binding studies. *Proc. Natl. Acad. Sci. USA* **1987**, *84*, 8922–8926.

(11) Portugal, J. and Waring, M. J., Assignment of DNA binding sites for 4',6-diamidine-2-phenylindole and bisbenzimide (Hoechst 33258). A comparative footprinting study. *Biochim. Biophys. Acta* **1988**, *949*, 158–168.

(12) Larsen, T. A.; Goodsell, D. S.; Cascio, D.; Grzeskowiak, K.; Dickerson, R. E., The structure of DAPI bound to DNA. *J. Biomol. Struct. & Dyn.* **1989**, *7*, 477–491.

(13) Tanious, F. A.; Veal, J. M.; Buczak, H.; Ratmeyer, L. S.; Wilson, W. D., DAPI (4',6-diamidino-2-phenylindole) binds differently to DNA and RNA: minor-groove binding at AT sites and intercalation at AU sites. *Biochemistry* **1992**, *31*, 3103–3112.

(14) Trotta, E.; D'Ambrosio, E.; Del Grosso, N.; Ravagnan, G.; Cirilli, M.; Paci, M., ^{1}H NMR study of $[d(GCGATCGC)]_2$ and its interaction with minor groove binding 4',6-diamidino-2-phenylindole. *J. Biol. Chem.* **1993**, *268*, 3944–3951.

(15) Wilson, W. D.; Tanious, F. A.; Barton, H. J.; Jones, R. L.; Fox, K.; Wydra, R. L.; Strekowski, L., DNA sequence dependent binding modes of 4',6-diamidino-2-phenylindole (DAPI). *Biochemistry* **1990**, *29*, 8452–8461.

(16) van Dyke, M. W. and Dervan, P. B., Echinomycin binding sites on DNA. *Science* **1984**, *225*, 1122–1127.

(17) Low, C. M.; Drew, H. R.; Waring, M. J., Sequence-specific binding of echinomycin to DNA: evidence for conformational changes affecting flanking sequences. *Nucleic Acid Res.* **1984**, *12*, 4865–4879.

(18) Ughetto, G.; Wang, A. H.; Quigley, G. J.; van der Marel, G. A.; van Boom, J. H.; Rich, A., A comparison of the structure of echinomycin and triostin A complexed to a DNA fragment. *Nucleic Acid Res.* **1985**, *13*, 2305–2323.

(19) Bailly, C.; Hamy, F.; Waring, M. J., Cooperativity in the binding of echinomycin to DNA fragments containing closely spaced CpG sites. *Biochemistry* **1996**, *35*, 1150–1161.

(20) Müller, W.; Crothers, D. M., Studies of the binding of actinomycin and related compounds to DNA. *J. Mol. Biol.* **1968**, *35*, 251–290.

(21) Sobell H. M.; Jain, S. C.; Sakore, T. D.; Nordman, C. E., Stereochemistry of actinomycin--DNA binding. *Nat. New Biol.* **1971**, *231*, 200–205.

(22) Lane, M.J.; Dabrowiak, J. C.; Vournakis, J. N., Sequence specificity of actinomycin D and Netropsin binding to pBR322 DNA analyzed by protection from DNase I. *Proc. Natl. Acad. Sci. USA* **1983**, *80*, 3260–3264.

(23) Chu, W.; Shinomiya, M.; Kamitori, K. Y.; Kamitori, S.; Carlson, R. G.; Weaver, R. F.; Takusagawa, F. *J. Am. Chem. Soc.* **1994**, *116*, 7971–7982.

(24) Trimmer, E. E.; Zamble, D. B.; Lippard, S. J.; Essigmann, J. M., Human testis-determining factor SRY binds to the major DNA adduct of cisplatin and a putative target sequence with comparable affinities. *Biochemistry* **1998**, 37, 352–362.

(25) Gelasco, A. and Lippard, S. J., NMR solution structure of a DNA dodecamer duplex containing a cis-diammineplatinum(II) d(GpG) intrastrand cross-link, the major adduct of the anticancer drug cisplatin. *Biochemistry* **1998**, *37*, 9230–9239.

(26) Takahara, P. M.; Rosenzweig, A. C.; Frederick, C. A.; Lippard, S. J., Crystal structure of double-stranded DNA containing the major adduct of the anticancer drug cisplatin. *Nature* **1995**, *337*, 649–652.

(27) van Boom, S. S.; Yang, D.; Reedijk, J.; van der Marel, G. A.; Wang, A. H., Structural effect of intra-strand cisplatin-crosslink on palindromic DNA sequences. *J. Biomol. Struct. Dyn.* **1996**, *13*, 989–998.

(28) Yang, D.; van Boom, S. S.; Reedijk, J.; van Boom, J. H.; Wang, A. H., Structure and isomerization of an intrastrand cisplatin-cross-linked octamer DNA duplex by NMR analysis. *Biochemistry* **1995**, *34*, 12912–12920.

(29) Kline, T. P.; Marzilli, L. G.; Live, D.; Zon, G., NMR studies of an oligonucleotide with an unusual structure induced by platinum anti-cancer drugs. *Biochem. Pharmacol.* **1990**, *40*, 97–113.

(30) Pil, P.; Lippard, S. J. "Cisplatin and related drugs" in Encyclopedia of Cancer edited by J.R. Bertino, pp.392–410, Academic Press, San Diego, C. A

(31) Sandman, K. E.; Marla, S. S.; Zlokarnik, G.; Lippard, S. J., Rapid fluorescence-based reporter-gene assays to evaluate the cytotoxicity and antitumor drug potential of platinum complexes. *Chemistry & Biology* **1999**, *6*, 541–555

(32) Ano, S. O.; Intini, F. P.; Natile, G.; Marzilli, L. G., A Novel Head-to-Head Conformer

of d(GpG) Cross-linked by Pt: New Light on the Conformation of Such Cross-links Formed by Pt Anticancer Drugs *J. Am. Chem. Soc.* **1998**, *120*, 12017–12022

(33) Hudson, B. P. and Barton, J. K., Solution Structure of a Metallointercalator Bound Site Specifically to DNA. *J. Am. Chem. Soc.* **1998**, *120*, 6877–6888

(34) Bailly, C. and Chaires, J. B., Sequence-specific DNA minor groove binders. Design and synthesis of netropsin and distamycin analogues. *Bioconj. Chem.* **1998**, *9*, 513–538.

(35) Trauger, K. W.; Baird, E. E.; Dervan, P. B., Recognition of DNA by designed ligands at subnanomolar concentrations. *Nature* **1996**, *382*, 559–561.

(36) Gottesfeld, J. M.; Neely, L.; Trauger, J. W.; Baird, E. E.; Dervan, P.B., Regulation of gene expression by small molecules. *Nature* **1997**, *387*, 202–205.

(37) Kielkopf, C. L.; White, S.; Szewczyk, J. W.; Turner, J. M.; Baird, E. E.; Dervan, P.B.; Rees, D. C., Structural effects of DNA sequence on T.A recognition by hydroxypyrrole/pyrrole pairs in the minor groove. *Science* **1998**, *282*, 111–115, and references therein.

(38) Shionoya, M.; Kimura, E.; Shiro, M., A new ternary zinc(II) complex with [12]aneN_4 (= 1,4,7,10-tetraazacyclododecane) and AZT (= 3'-azido-3'-deoxythymidine). Highly selective recognition of thymidine and its related nucleotides by a zinc(II) macrocyclic tetraamine complex with novel complementary association. *J. Am. Chem. Soc.* **1993**, *115*, 6730–6737.

(39) Shionoya, M.; Ikeda, T.; Kimura, E.; Shiro, M., Novel "multipoint" molecular revognition of nucleobases by a new zinc(II) complex of acridine-pendant cyclen (cyclen = 1,4,7,19-tetraazacyclododecane). *J. Am. Chem. Soc.* **1994**, *116*, 3848–3859.

(40) Kimura, E.; Ikeda, T.; Shionoya, M., Macrocyclic metal complexes for selective recognition of nucleic acid bases and manipulation of gene expression. *Pure & Appl. Chem.* **1997**, *69*, 2187–2195.

(41) Kimura, E.; Ikeda, T.; Aoki, S.; Shionoya, M., Macrocyckic ainc(II9 complexes for selective recognition of nucleobases in single- and double-stranded polynucleotides. *J. Biol. Inorg. Chem.* **1998**, *3*, 259–267.

(42) Kimura, E.; Kikuchi, M.; Kitamura, H.; Koike, T., Selective and efficient recognition of

thymidylthymidine (TpT) by bis(Zn^{2+}-cyclen) and thymidylthymidylthymideine (TpTpT) by tris(Zn^{2+}-cyclen) at neutral pH in aqueous solution. *Chem. Eur. J.* **1999**, *5*, 3113-3123

(43) Kimura, E.; Kitamura, H.; Ohtani, K.; Koike, T., Elaboration of Selective and Efficient Recognition of Thymine Base in Dinucleotides (TpT, ApT, CpT, and GpT), Single-Stranded d(GTGACGCC), and Double-Stranded $d(CGCTAGCG)_2$ by Zn^{2+}-Acridinylcyclen (Acridinylcyclen = (9-Acridinyl)methyl-1,4,7,10-tetraazacyclen. *J. Am. Chem. Soc.* **2000**, *122*, 4668–4677

(44) Galas, D. J. and Schmitz, A., DNAse footprinting: a simple method for the detection of protein-DNA binding specificity. *Nucleic. Acids. Res.* **1978**, *5*, 3157–3170.

(45) Fox, K. R. and Warning, M. J., The use of micrococcal nuclease as a probe for drug-binding sites on DNA. *Biochim. Biophys. Acta* **1987**, *909*, 145–155.

(46) Drew, H. R., Structural specificities of five commonly used DNA nucleases. *J. Mol. Biol.* **1984**, *176*, 535–557.

(47) Tucker, J. H. R.; Shionoya, M.; Koike, T.; Kimura, E., a zinc(II)-cyclen complex attached to an anthraquinone moiety that acts as a redox-active nucleobase receptor in aqueous solution. *Bull. Chem. Soc. Jpn* **1995**, *68*, 2465–2469.

(48) Koike, T.; Gotoh, T.; Aoki, S.; Kimura, E.; Shiro, M., A new macrocyclic tetraamine, 2,4-dinitrophenylcyclen (=1-(2,4-dinotrophenyl)-1,4,7,10-tetraazacyclododecane): synthesis, cation reporter properties, and recognition of 1-methylthymine by its zinc(II) complex. *Inorg. Chim. Acta* **1998**, *270*, 424–432.

(49) A similiar method for the determination of conditional affinity constants for imide-deprotonated barbital complexes with Zn^{2+}–cyclen derivatives at pH 8 was previously reported: Fujioka, H.; Koike, T.; Yamada, N.: Kimura, W., A new bis(Zinc(II)-cyclen) complex s a novel chelator for barbiturates and phosphates. *Heterocycles* **1996**, *42*, 775–787.

(50) Significantly larger complexation constants with dT^- (or U^-) (see Table 1) and the ^1H NMR data (e.g., a large upfield shift of thymine H(6) in dT^-–**13** (δ 7.12 at pD 8.5) from uncomplexed dT^- (δ 7.50 at pD >12)) suggest that the aromatic rings in **13** and **15** act as

bis-intercalators to sandwich thymine group.

(51) Lokey, R. S.; Kwok, Y.; Guelev, V.; Pursell, C. J.; Hurley, L. H.; Iverson, B. L., A New Class of Polyintercalating Molecules. *J. Am. Chem. Soc.* **1997**, *119*, 7202–7210.

(52) Tullius, T. D., DNA footprinting with hydroxyl radical. *Nature* **1988**, *332*, 663–664.

(53) Aoki, S.; Honda, Y.; Kimura, E., The First Selective and Efficient Transport of Imide-Containing Nucleosides and Nucleotides by Lipophilic Cyclen-Zinc(II) Complexes (Cyclen = 1,4,7,10-Tetraazacyclododecane) *J. Am. Chem. Soc.* **1998**, *120*, 10018–10026.

(54) Aoki, S.; Sugimura, C.; Kimura, E., Efficient Inhibition of Photo[2 + 2]cycloaddition of Thymidilyl(3'-5')thymidine and Promotion of Photosplitting of the cis-syn-Cyclobutane Thymine Dimer by Dimeric Zinc(II)-Cyclen Complexes Containing m- and p-Xylyl Spacers, *J. Am. Chem. Soc.* **1998**, *120*, 10094–10102.

(55) Kimura, E. and Koike, T., Dynamic Anion Recognition by Macrocyclic Polyamines in Neutral pH Aqueous Solution: Development from Static Anion Complexes to an Enolate Complex. *J. Chem. Soc. Chem. Commun.* **1998**, 1495–1500.

(56) Kimura, E., Distinctive coordination chemistry and biological relevance of complexes with macrocyclic oxo polyamines. *J. Coord. Chem.* **1986**, *15*, 1–28.

(57) Kodama, M. and Kimura, E., A thermodynamic and kinetic interpretation of the macrocyclic eddect. Polarographic studies on copper(II) 1,4,7,10-tetraazacyclododecane complexation. *J. Chem. Soc. Chem. Comm.* **1975**, 326–327.

(58) Kodama, M. and Kimura, E., Equilibria and kinetics of complexes formation between zinc(II), lead(II) and cadmium(II), and 12-, 13-, 14-, and 15-membered macrocyclic tetraamines. *J. Chem. Soc. Dalton. Trans.* **1977**, 2269–2276.

(59) Koike, T.; Takamura, M.; Kimura, E., Role of zinc(II) in β-lactamase II: a model study with a zinc(II)-macrocyclic tetraamine (1,4,7,10-tetraazsacyclododecane, cyclen) complex *J. Am. Chem. Soc.* **1994**, *116*, 8443–8449.

(60) Zimmermann, H. W., Physiological and cytochemical investigations on the binding of ethidium and acridine dyes to DNA and to organelles in living cells. *Angew. Chem. Int. Ed. Engl.* **1986**, *25*, 115-130

(61) Kumar, C. V. and Asuncion, E. H., DNA binding studies and site selective fluorescence sensitization of an anthryl probe. *J. Am. Chem. Soc.*, **1993**, *115*, 8547–8553

(62) Kim, S. K. and Nordén, B., Methyl green. A DNA major-groove binding drug. *FEBS letter* **1993**, *315*, 61-64

(63) Fox, K. R.; Higson, S. L.; Scott, J. E., Methyl green and its analogues bind selectively to AT-rich regions of native DNA. *Eur. J. Histochem.* **1992**, *36*, 263-270

(64) Tuite, E.; Sehlstedt, U.; Hagmer, P.; Norden, B.; Takahashi, M., Effects of minor and major groove-binding drugs and intercalators on the DNA association of minor groove-binding proteins RecA and deoxyribonuclease I detected by flow linear dichroism. *Eur. J. Biochem.* **1997**, *243*, 482-492

(65) Kumar, K.A. and Muniyappa, K., Use of structure-directed DNA ligands to probe the binding of recA protein to narrow and wide grooves of DNA and on its ability to promote homologous pairing. *J. Biol. Chem.* **1992**, *267*, 24824-24832

(66) Latt, S. A., , Optical studies of metaphase chromosome organization. *Annu. Rev. Biophys. Bioeneng.* **1976**, *5*, 1-37

(67) Wang, J. C. DNA topoisomerases. *Annu. Rev. Biochem.* **1985**, *54*, 665-697

(68) Chen, A. Y.; Yu, C.; Gatto, B.; Liu, L. F., DNA minor groove-binding ligands: a different class of mammalian DNA topoisomerase I inhibitors. *Proc. Natl. Acad. Sci. USA* **1993**, *90*, 8131-8135

(69) Mortensen, U. H.; Stevnsner, T.; Krogh, S.; Olsen, K.; Westergaard, O.; Bonven, B., Distamycin inhibition of topoisomerase I-DNA interaction: a mechanistic analysis. *Nucleic Acids Res.* **1990**, *18*, 1983-1989

(70) McHugh, M. M.; Woynarowski, J. M.; Sigmund, R. D.; Beerman, T. A., Effect of minor groove binding drugs on mammalian topoisomerase I activity. *Biochem. Pharmacol.* **1989**, *38*, 2323-2328

(71) Woynarowski, J. M.; McHugh, M. M.; Sigmund, R. D.; Beerman, T. A., Modulation of topoisomerase II catalytic activity by DNA minor groove binding agents distamycin, Hoechst 33258, and 4',6-diamidine-2-phenylindole. *Mol. Pharmacol.* **1988**, *35*, 177-8135

(72) Bucher, P., Weight matrix descriptions of four eukaryotic RNA polymerase II promoter elements derived from 502 unrelated promoter sequences. *J. Mol. Biol.* **1990**, *212*, 563-578

(73) Sharp, P., TATA binding protein is a classless factor. *Cell* **1992**, *68*, 819-821

(74) Bellorini, M.; Moncollin, V.; D'lncalci, M.; Mongelli, N.; Mantovani, R., Distamycin A and tallimustine inhibit TBP binding and basal in vitro transcription. *Nucleic Acids Res.* **1995**, 23, 1657-1663

(75) Chiang, S.; Welch, J.; Rauscher III, F. J.; Beerman, T. A., Effects of minor groove binding drugs on the interaction of TATA box binding protein and TFIIA with DNA. *Biochemistry* **1994**, *33*, 7033-7040

(76) Hansen, M.; Lee, S-J.; Cassady, J. M.; Hurley, L. H., Molecular Details of the Structure of a Psorospermin-DNA Covalent/Intercalation Complex and Associated DNA Sequence Selectivity. *J. Am. Chem. Soc.* **1996**, 118, 5553–5561

(77) David, T. B. and Schuster, G. B., Anthraquinone Photonucleases: Mechanisms for GG-Selective and Nonselective Cleavage of Double-Stranded DNA. *J. Am. Chem. Soc,* **1996**, *118*, 2311–2319

(78) Armitage, B.; Yu, C.; Devadoss, C.; Schuster, G. B. *J. Am. Chem. Soc.* **1994**, *116*, 9847–9859

(79) Gasper, S. M. and Schuster, G. B., Intramolecular Photoinduced Electron Transfer to Anthraquinones Linked to Duplex DNA: The Effect of Gaps and Traps on Long-Range Radical Cation Migration. *J. Am. Chem. Soc.* **1997**, *119*, 12762–12771

(80) Gasper, S. M. and Schuster, G. B., Three-Dimensional Structure and Reactivity of a Photochemical Cleavage Agent Bound to DNA. *J. Am. Chem. Soc.* **1998**, *120*, 12402–12409

(81) Qu, X. and Chaires J. B., Contrasting Hydration Changes for Ethidium and Daunomycin Binding to DNA. *J. Am. Chem. Soc.* **1999**, *121*, 2649–2650

(82) Sun, D.; Thompson, B.; Cathers, B. E.; Salazar, M.; Kerwin S. M.; Trent, J. O.; Jenkins, T. C.; Niedle, S.; Hurley, L. H., Inhibition of human telomerase by a G-quadruplex-interactive compound. *J. Med. Chem.* **1997**, *40*, 2113–2116

(83) Perry, P. J.; Reszka, A. P.; Wood, A. A.; Read, M. A.; Gowan, S. M.; Dosanjh, H. S.; Trent, J. O.; Jenkins, T. C.; Kelland, L. R.; Niedle, S., Human telomerase inhibition by regioisomeric disubstituted amidoanthracene-9,10-diones. *J. Med. Chem.* **1998**, *41*, 4873–4884

(84) Fox, K. R.; Waring, J. R.; Niedle, S., DNA sequence preferences for the anti-cancer drug mitoxanthrone and related anthraquinones revealed by DNase I footprinting. *FEBS letter* **1986**, *202*, 289-294

(85) Hsieh, H. P.; Muller, J. G.; Burrows, C., Structual effects in nocel steroidal polyamine-DNA binding. *J. Am. Chem. Soc.* **1994**, *116*, 12077–12078

(86) Sartorious, J. and Schneider, H. J., Intercalation mechanisms with ds-DNA: binding modes and energy contributions with benzene, naphtalenem qionoline and indole derivatives including some antimalalials *J. Chem. Soc. Perkin Trans.* **1997**, *2*, 2319-2327

(87) Bresloff J. L. and Crothers, D.M., Equilibrium studies of ethidium--polynucleotide interactions. *Biochemistry* **1981**, *20*, 3547-3553

(88) Dynan, W. S. and Tijian, R., Isolation of transcription factors that discriminate between different promoters recognized by RNA polymerase II. *Cell* **1983**, *32*, 669–680

(89) Kadonaga, J. T.; Carner, K. R.; Masiarz, F. R.; Tijian, R., Isolation of cDNA encoding transcription factor Sp1 and functional analysis of the DNA binding domain. *Cell* **1987**, *51*, 1079–1090

(90) Elrod-Elickson, M.; Rould, M. A.; Nekludova, L.; Pabo, C. O., Zif268 protein-DNA complex refined at 1.6 A: a model system for understanding zinc finger-DNA interactions. *Structure* **1996**, *4*, 1171–1180

(91) Yokono, M.; Saegusa, N.; Matsushita, K.; Sugiura, Y., Unique DNA binding mode of the N-terminal zinc finger of transcription factor Sp1. *Biochemistry* **1998**, *37*, 6824–6832

(92) Wells, R.D.; Larson, J. E.; Grant, R. C.; Shortle, B. E.; Cantor, C. R., Physicochemical studies on polydeoxyribonucleotides containing defined repeating nucleotide sequences. *J. Mol. Biol.* **1970**, *54*, 465-497

(93) Inman, R. B. and Baldwin, R. L., Helix-random coil transitions in synthetic DNAs of alternating aequence. *J. Mol. Biol.* **1962**, *5*, 172-184

(94) Inman, R. B. and Baldwin, R. L., Helix-random coil transitions in DNA homopolymer airs. *J. Mol. Biol,* **1964**, *8*, 452-469

(95) Grant, R. C.; Harwood, S. J.; Wells, R. D., The synthesis and characteriztion of poly d(I-C)·polyd(I-C). *J. Am. Chem. Soc.* **1968**, *90*, 4474-4476

(96) Chamberlin, M. J., Comparative properties of DNA, RNA, and hybrid homopolymer pairs. *Fed. Proc.* **1965**, *24*, 1446-1457

(97) Ts'o, P. O.; Rapaport, S. A.; Bollum, F. J., A comparative study of polydeoxyribonucleotides and polyribenucleotides by optical ratatory dispersion. *Biochemistry* **1966**, *5*, 4153-4170

(98) Dumont, A.; Jacques, V.; Desreux, J.F., Regioselective synthesis of 1,7-diprotected 1,4,7,10-tetraazacyclododecane and preparation of a dialcohol dicarboxylic macrocyclic ligand. *Tetrahedron Lett.* **1994**, *35*, 3703–3710

(99) Kimura, E.; Aoki, S.; Koike, T.; Shiro, M., A Tris(ZnII-1,4,7,10-tetraazacyclododecane) Complex as a New Receptor for Phosphate Dianions in Aqueous Solution. *J. Am. Chem. Soc.* **1997**, *119*, 3068-3076

(100) Maxam, A. M. and Gilbert, W., A new method for sequencing DNA. *Proc. Natl. Acad. Sci. USA* . **1977**, *74*, 560–564

(101) Chaires, J. B.; Dattagupta, N.; Crothers, D. M., Self-association of daunomycin. *Biochemistry* **1982**, *21*, 3933-3940

List of Original Articles and Reviews

1. Original Articles

(1) Emiko Kikuta, Mariko Murata, Naomi Katsube, Tohru Koike, and Eiichi Kimura
Novel Recognition of Thymine Base in Double-Stranded DNA by Zinc(II)-Macrocyclic Tetraamine Complexes Appended with Aromatic Groups.
J. Am. Chem. Soc., **1999**, 121, 5426–5436

(2) Emiko Kikuta, Naomi Katsube, and Eiichi Kimura
Natural and Synthetic Double-Stranded DNA Binding Studies of Macrocyclic Tetraamine Zinc(II) Complexes Appended with Polyaromatic Groups.
J. Biol. Inorg. Chem., **1999**, 4, 431–440

(3) Emiko Kikuta, Tohru Koike, and Eiichi Kimura
Controlling Gene Expression by Zinc(II)-Macrocyclic Tetraamine Complexes.
J. Inorg. Biochem., **2000**, 79, *253-259*

(4) Emiko Kikuta, Reiko Matsubara, Naomi Katsube, Tohru Koike, and Eiichi Kimura
Selective Recognition of Consecutive G Sequence in Double-Stranded DNA by a Zinc(II)–Macrocyclic Tetraamine Complex Appended with an Anthraquinone.
J. Inorg. Biochem., **2000**, 82, 239-249

2. Reviews

(1) Eiichi Kimura and Emiko Kikuta
Why Zinc in Zinc Enzymes? From Biological Roles to DNA Base–Selective Recognition.
J. Biol. Inorg. Chem., **2000**, 5, 139-155

(2) Eiichi Kimura and Emiko Kikuta
Macrocyclic Zinc(II) Complexes for Selective Recognition of Nucleobases in Single- and Double-Stranded Polynecleotides.
Progress in Reaction Mechanism and Kinetics, **2000**, 25, 1–64

Acknowledgement

本研究を遂行するにあたり、完全な研究環境と、常に適格な御指導をいただきました、広島大学医学部総合薬学科　木村榮一　教授に慎んで感謝と敬意を表します。

本研究において、数々の御指導、助言をいただきました、広島大学医学部総合薬学科　小池　透　教授、青木　伸　助教授、本論文指導委員として御指導をいただきました　武田　敬　教授、杉山　政則　教授　をはじめ、薬学科の諸先生方に深く感謝致します。

本研究は多くの方々の支援によって成し得たものであることをここに銘記し、お世話になりました皆様に心より感謝いたします。

平成 13 年 6 月